TKK Dissertations 201
Espoo 2009

INSTRUMENTATION AND METHODS FOR FREQUENCY-DOMAIN AND MULTIMODAL NEAR-INFRARED SPECTROSCOPY

Doctoral Dissertation

Tommi Noponen

Helsinki University of Technology
Faculty of Information and Natural Sciences
Department of Biomedical Engineering and Computational Science

TKK Dissertations 201
Espoo 2009

INSTRUMENTATION AND METHODS FOR FREQUENCY-DOMAIN AND MULTIMODAL NEAR-INFRARED SPECTROSCOPY

Doctoral Dissertation

Tommi Noponen

Dissertation for the degree of Doctor of Science in Technology to be presented with due permission of the Faculty of Information and Natural Sciences for public examination and debate in Auditorium F239a at Helsinki University of Technology (Espoo, Finland) on the 11th of December, 2009, at 12 noon.

Helsinki University of Technology
Faculty of Information and Natural Sciences
Department of Biomedical Engineering and Computational Science

Teknillinen korkeakoulu
Informaatio- ja luonnontieteiden tiedekunta
Lääketieteellisen tekniikan ja laskennallisen tieteen laitos

Distribution:
Helsinki University of Technology
Faculty of Information and Natural Sciences
Department of Biomedical Engineering and Computational Science
P.O. Box 2200 (Rakentajanaukio 2)
FI - 02015 TKK
FINLAND
URL: http://www.becs.tkk.fi/
Tel. +358-9-470 23172
Fax +358-9-470 23182
E-mail: tommi.noponen@tkk.fi

ISBN 978-952-248-210-5
ISBN 978-952-248-211-2 (PDF)
ISSN 1795-2239
ISSN 1795-4584 (PDF)
URL: http://lib.tkk.fi/Diss/2009/isbn9789522482112/

TKK-DISS-2684

Painosalama Oy
Turku 2009

ABSTRACT OF DOCTORAL DISSERTATION	HELSINKI UNIVERSITY OF TECHNOLOGY P. O. BOX 1000, FI-02015 TKK http://www.tkk.fi

Author Tommi Noponen

Name of the dissertation

Instrumentation and methods for frequency-domain and multimodal near-infrared spectroscopy

Manuscript submitted August 24, 2009	Manuscript revised November 6, 2009
Date of the defence December 11, 2009	
☐ Monograph	☒ Article dissertation (summary + original articles)

Faculty	Faculty of Information and Natural Sciences
Department	Department of Biomedical Engineering and Computational Science
Field of research	Biomedical Engineering
Opponent(s)	Professor Sergio Fantini, Tufts University
Supervisor	Professor Pekka Meriläinen
Instructor	Timo Kajava, D.Sc. (Tech.)

Abstract

In this thesis, instrumentation for a frequency-domain (FD) near-infrared spectroscopy (NIRS) device and for multimodal brain measurements was implemented. Different techniques were applied to human and newborn lamb brain studies. A method to detect light leakage in NIRS measurements was developed.

The FD instrument, developed at the Helsinki University of Technology was extended, by implementing 16 pseudo-differential preamplifiers for the analog-to-digital converters with a low noise and excellent interchannel isolation. An instrumentation for a digital signal-processor based lock-in amplifier was also developed. Methods for increasing the number of wavelengths and source positions in the imaging instrument were studied. A second-generation source system with a fast fiber-optic switch and four high-power laser diodes with a low noise temperature-stabilizing electronics was implemented. The imaging device was placed into a cabinet to enable its portability. New detection and source fiber terminals were developed for multimodal brain studies.

The different versions of the imaging instrument were applied to four human brain measurements. In a breath-holding and hyperventilation study, the effects of source-detector distance (SDD) and measurement wavelength on the contrast of NIRS responses and the frequency content of signals were studied. Hemodynamic changes in the human brain related to the changes in sleep stages were detected. The multimodal NIRS and electroencephalography measurement setup was implemented and used to study the effects of baseline blood flow changes on the visually evoked hemodynamic and neuronal responses. The feasibility of NIRS as a part of multimodal monitoring setup to detect cerebral hemodynamic changes induced by iloprost and nitric oxide in the preterm lamb brain was also demonstrated.

The linearity of the FD measurement parameters as a function of SDD on the human forehead was studied. The regression of phase measurement was observed to be sensitive to light leakage from source to detectors, much more than the regression of modulation amplitude or average intensity measurement. Utilizing this observation, a method to detect light leakage based on the pathlength measurement was developed. The contrast and depth sensitivity of NIRS signals were shown to decrease in measurements where light leakage occurs.

Keywords	near-infrared spectroscopy, frequency-domain technique, light leakage, multimodal brain measurement
ISBN (printed) 978-952-248-210-5	ISSN (printed) 1795-2239
ISBN (pdf) 978-952-248-211-2	ISSN (pdf) 1795-4584
Language English	Number of pages 82 p. + app. 134 p.
Publisher	Helsinki University of Technology, Department of Biomedical Engineering and Computational Science
Print distribution	Helsinki University of Technology, Dep. of Biomedical Engineering and Computational Science

☒ The dissertation can be read at http://lib.tkk.fi/Diss/2009/isbn9789522482112/

VÄITÖSKIRJAN TIIVISTELMÄ	TEKNILLINEN KORKEAKOULU PL 1000, 02015 TKK http://www.tkk.fi

Tekijä Tommi Noponen

Väitöskirjan nimi

Laitetekniikkaa ja menetelmiä taajuusalueen lähi-infrapunaspektroskopiaan ja monimenetelmätutkimuksiin

Käsikirjoituksen päivämäärä 24.8.2009	Korjatun käsikirjoituksen päivämäärä 06.11.2009
Väitöstilaisuuden ajankohta 11.12.2009	
☐ Monografia	☒ Yhdistelmäväitöskirja (yhteenveto + erillisartikkelit)

Tiedekunta	Informaatio- ja luonnontieteiden tiedekunta
Laitos	Lääketieteellisen tekniikan ja laskennallisen tieteen laitos
Tutkimusala	Lääketieteellinen tekniikka
Vastaväittäjä(t)	Professori Sergio Fantini, Tufts University
Työn valvoja	Professori Pekka Meriläinen
Työn ohjaaja	Timo Kajava, TkT

Tiivistelmä

Työssä kehitettiin laitetekniikkaa ja menetelmiä taajuusalueen lähi-infrapunaspektroskopiaan (NIRS) ja monimenetelmätutkimuksiin. Menetelmiä sovellettiin aivomittauksiin ihmisillä ja vastasyntyneillä lampailla. Työssä kehitettiin myös menetelmä valovuodon havaitsemiseen otsamittauksissa.

Teknillisessä korkeakoulussa kehitettyä taajuusalueen laitetta laajennettiin toteuttamalla laitteeseen 16 vähäkohinaista analogi-digitaalimuuntimen etuvahvistinta, joiden kanavien välinen ylikuuluminen on erittäin vähäistä. Työn aikana kehitettiin signaaliprosessoritekniikkaan perustuva nelikanavainen vaihelukittu vahvistin. Taajuusalueen laitteen aallonpituuksien ja lähdekanavien määrän lisäämiseen liittyviä tekniikoita tutkittiin. Työssä kehitettiin myös nopeaan kuitukytkimeen ja neljään suuritehoiseen lämpötilasäädeltyyn laserdiodiin perustuva lähdejärjestelmä. Kuvantamislaite asennettiin laitetelineeseen sen siirrettävyyden helpottamiseksi. Lisäksi lähde- sekä vastaanotinkuituihin kehitettiin uudet päätteet monimenetelmäisiä aivomittauksia varten.

Kuvantamislaitteen eri kehitysversioita käytettiin ihmisillä neljässä aivotutkimussarjassa. Lähde-ilmaisinetäisyyden ja mittausaallonpituuden vaikutusta signaaleihin ja signaalien taajuussisältöä tutkittiin ylihengitys- ja hengityksenpidätysmittauksissa. Otsamittauksissa havaittiin unitasoihin liittyviä hemodynaamisia muutoksia. Työssä kehitetyllä järjestelmällä tutkittiin aivojen verenvirtauksen perustasonmuutosten ja näköärsykkeillä synnytettyjen hemodynaamisten tai sähköisten vasteiden välisiä yhteyksiä. Osana monimenetelmäistä monitorointijärjestelmää NIRS:llä mitattiin myös hengitetyn iloprostin ja typpioksidin synnyttämiä hemodynaamisia muutoksia vastasyntyneen lampaan aivoissa.

Työssä tutkittiin myös taajuusalueen mittausparametrien lineaarisuutta otsamittauksissa. Vaihemittauksen havaittiin olevan selvästi herkempi ilmaisemaan mahdollisia valovuotoja kuin intensiteetti- tai amplitudimittaus. Tähän havaintoon perustuen työssä kehitettiin menetelmä valovuotojen havaitsemiseen. Signaalien kontrastin ja syvyysherkkyyden osoitettiin laskevan selvästi mittauksissa, joissa havaittiin valovuotoa.

Asiasanat	Lähi-infrapunaspektroskopia, taajuusalueen tekniikka, valovuoto, monimenetelmäiset aivotutkimukset	
ISBN (painettu)	978-952-248-210-5	ISSN (painettu) 1795-2239
ISBN (pdf)	978-952-248-211-2	ISSN (pdf) 1795-4584
Kieli	Englanti	Sivumäärä 82 s. + liit. 134 s.
Julkaisija	Teknillinen korkeakoulu, Lääketieteellisen tekniikan ja laskennallisen tieteen laitos	
Painetun väitöskirjan jakelu	Teknillinen korkeakoulu, Lääketieteellisen tekniikan ja laskennallisen tieteen laitos	
☒ Luettavissa verkossa osoitteessa http://lib.tkk.fi/Diss/2009/isbn9789522482112/		

To Pirkko, Kaarlo, Tuomo and Alpo

Preface

Much of this work was carried out at the Laboratory of Biomedical Engineering at the Helsinki University of Technology (HUT) and at the BioMag Laboratory at the Helsinki University Central Hospital during the years 2001 - 2006. At that time both laboratories belonged to the Helsinki Brain Research Center (HBRC). I would like to thank my supervisor Professor Pekka Meriläinen for encouraging me to finish this thesis and to study other physiological monitoring techniques in addition to NIRS, and for deepening my knowledge of the biomedical engineering industry. I wish to express my gratitude to my former supervisor Emeritus Professor Toivo Katila for providing me with excellent research facilities and creating such a highly fascinating institute for biomedical engineering education. Topi's lab was a good place to professionally mature. To Professor Vineta Fellman I express my sincere gratitude for providing me with a highly vital impulse to complete this thesis and for all the guidance in the world of statistics and pediatrics. My instructor Dr.Tech. Timo Kajava is greatly acknowledged for very diligently advising me to gain better skills on scientific writing and for carefully revising this thesis. Without your help Timo, this thesis would have been much more difficult to understand. I also wish to thank the pre-examiners of this thesis Professors Brian Pogue and Pekka Hänninen for their improving comments and corrections, and Ph.D. Tony Shepherd for checking the language of my manuscript.

Many parts of this thesis were carried out together with other researchers in the Medical Optical Imaging (MOI) group at HUT. I express my gratitude to Dr.Tech. Ilkka Nissilä for his creative ideas and enthusiasm, which enabled us to develop such an excellent tomographic instrument. Ilkka also deserves a great acknowledgement for being the corresponding author of the two first publications of this thesis. I wish to thank M.Sc. Kalle Kotilahti and M.Sc. Lauri Lipiäinen for contributing essentially to our instrumentation and methodological development and for being such great friends during all these years. I thank Dr.Tech. Jenni Heino and Dr.Tech. Juha Heiskala for deepening my knowledge on the modeling of optical tomography and Jenni for contributing essentially to Publication I of this thesis. The current group members M.Sc. Tiina Näsi, M.Sc. Jaakko Virtanen, and M.Sc. Petri Hiltunen are greatly acknowledged for their inspiring attitude toward the research and for their friendship during the last years of this project. I see in you the promising future of medical optical imaging research in Finland. Also, I wish to thank all current and former members of MOI group such as Maunu, Nasia, Riikka, Mauro, Lidet, and Atte for their contributions to the advancement of our research.

I express my gratitude to Professor Simon Arridge and Ph.D. Tanja Tarvainen for their long lasting collaboration with our group and contributions to this thesis. Docent Tapani Salmi and Dr. Jussi Toppila are acknowledged for their advice and contributions in our sleep studies and Dr.Tech. Dubravko Kičić for helping me in the multichannel EEG studies and for those memorable moments when we advertised

the novel biomedical techniques within the HBRC. I also wish to thank the other co-authors M.D. Anders Nordh, Ph.D. Martin Schweiger, Docent Seppo Kähkönen, Ass. Professor Ansgar Berg, Ph.D. David Ley, Docent Stefan Hansson, and Professor Erkki Pesonen for their contributions to this thesis. Especially, I express my sincere gratitude to Anders for showing such unselfishness during the final stage of our publication.

I would like to thank Doc. Minna Huotilainen for her important collaboration with our group and Professor Risto Näätänen for being interested in NIRS research and financially supporting us through the HBRC. I thank also Professor Risto Ilmoniemi for exhorting me to finally finish this thesis. Professor Ari Koskelainen and Professor Matti Kaivola are acknowledged for showing interest in my work, especially in its early phase and Matti for advising me on my journeys in the world of optics. I express my gratitude to Assistant chief physicist Mika Teräs and Professor Juhani Knuuti for providing me with the time during the last couple of months to complete this dissertation. Without that understanding my thesis may not be ready yet. Chief physicist Jarmo Kulmala is acknowledged for showing interest in my work and encouraging me to finish it. I would also like to thank Hospital physicist Tuula Tolvanen, M.Sc. Pauliina Luoto, M.Sc. Tommi Kokki, and Ph.D. Riku Klén, all the radiographers, medical laboratory technologies, researchers, professors, and other staff in the Turku PET Centre for creating such a friendly working environment and for showing their understanding during my last steps in this project. I also gratefully acknowledge the following funding agencies; the Finnish Foundation for Technology Promotion, the Jenny and Antti Wihuri Foundation, the Emil Aaltonen Foundation, the Instrumentarium Foundation, the Finnish Cultural Foundation, the Finnish Funding Agency for Technology and Innovation, and the Academy of Finland for their financial support during this work.

I wish to thank with all my heart my dear parents Kati and Arto for all your support and encouragement during my long trip to achieve the doctor's degree. Without your recent help in babysitting, house remodeling and several other practical matters, this work would definitely have been delayed even more. I thank my brother Jimi for teaching me the order of importance in life. I wish to thank also my parents-in-law Kalle and late Seija for always highly respecting my work. Seija's heartfelt and helpful character will always last in our memories. Finally, more than anyone else I wish to thank my beautiful, loving wife Pirkko and our adorable sons, young gentleman Kaarlo, Tuomo living in the moment, and fantasy-traveller Alpo. I am greatly indebted to you for all the time I have spent in finishing this dissertation. I will try with all my best to pay those lost moments back to you. You are the most valuable treasures in my life.

Kaarina, November 2009

Tommi Noponen

Contents

List of Publications

This thesis consists of an overview and the following six publications.

I I. Nissilä, T. Noponen, J. Heino, T. Kajava, and T. Katila. Diffuse optical imaging. In J. C. Lin (ed.), *Advances in Electromagnetic Fields in Living Systems*, vol. **4**, Springer Science+Business Media, New York, 2005, pp. 77−129.

II I. Nissilä, T. Noponen, K. Kotilahti, T. Tarvainen, M. Schweiger, L. Lipiäinen, S. Arridge, and T. Katila. Instrumentation and calibration methods for the multichannel measurement of phase and amplitude in optical tomography. *Review of Scientific Instruments*, **76**(4), article 044302 (10 pages), 2005.

III T. Noponen, K. Kotilahti, J. Toppila, I. Nissilä, T. Salmi, T. Kajava, and T. Katila. Near-infrared measurements of hemodynamic and oxygenation changes on the frontal cortex during breath holding, hyperventilation, and natural sleep. In B. Chance, R. R. Alfano, B. J. Tromberg, M. Tamura, E. M. Sevick-Muraca (eds.), *Proc. SPIE* **4955**, 2003, pp. 124-133.

IV T. Noponen, D. Kičić, K. Kotilahti, T. Kajava, S. Kähkönen, I. Nissilä, P. Meriläinen, and T. Katila. Simultaneous diffuse near-infrared imaging of hemodynamic and oxygenation changes and electroencephalographic measurements of neuronal activity in the human brain. In B. Chance, R. R. Alfano, B. J. Tromberg, M. Tamura, E. M. Sevick-Muraca (eds.), *Proc. SPIE* **5693**, 2005, pp. 179-190.

V T. Noponen, A. Nordh, A. Berg, D. Ley, S.R. Hansson, E. Pesonen, and V. Fellman. Circulatory effects of inhaled iloprost in the newborn preterm lamb. *Pediatric Research* **66**(4):416-422, 2009.

VI T. Noponen, K. Kotilahti, I. Nissilä, T. Kajava, and P. Meriläinen. Effects of improper source coupling in frequency-domain near-infrared spectroscopy. *Helsinki University of Technology Publications in Engineering Physics*, Report TKK-F-**A859**, 20 pages, 2009.

Throughout the overview these publications are referred by their Roman numerals.

Author's contribution

The six original articles included in this thesis are the result of collaborative work. In all these studies the author has had a significant role as described in detail below.

Publication I is an extensive book chapter reviewing diffuse optical imaging and especially tomographic techniques. The author wrote Sects. 2 (Tissue optics and physiology), 5.1 (Muscle studies), and 5.2 (Optical mammography) and a part of the discussion section and contributed in the writing of the abstract and the introduction. He also gave comments, references, and made corrections to the other sections.

Publication II introduces instrumentation and calibration methods of the multichannel frequency-domain instrument. The author designed and implemented the IF preamplifiers, a substantial part of the source and wavelength switching techniques, proposed improvements to the temperature stabilizer electronics, helped in the implementation of the RF electronics, contributed to the development of the software lock-in amplifier (LIA) and the control software, participated in testing of the instrument, and implemented some alternative parts such as a four-channel digital LIA. He also participated in the writing of the manuscript by giving comments, suggestions, and making corrections.

For Publications III, IV and VI, the author designed the study series, applied the permissions, made most of the measurements except the EEG measurements of Publication IV and the calibration measurement of Publication VI. He implemented all the signal processing algorithms except the calibration algorithm of Publication VI and processed the data except the sleep classification of Publication III and the preprocessing and averaging of EEG signals of Publication IV. The author analysed all the results and wrote the manuscripts. He also invented the coupling error detection method of Publication VI.

For Publication V, the author contributed to the design of the near-infrared spectroscopy (NIRS) study part and the acquisition of NIRS data. He was responsible for analysing the NIRS data and also analysed the other preprocessed data. The manuscript was written in collaboration with all the authors.

List of Abbreviations

AC	alternating current
A/D	analog-to-digital
A.U.	arbitrary unit
AUC	area-under-the-curve
BOLD	blood oxygen level-dependent
bpm	beats per minute
CBF	cerebral blood flow
CBV	cerebral blood volume
CC	correlation coefficient
CF	carotid flow
$CMRO_2$	cerebral metabolic rate of oxygen
CNR	contrast-to-noise ratio
CO_2	carbon dioxide
CSF	cerebrospinal fluid
CW	continuous wave
Cyto-Ox	cytochrome oxidase
dB	decibel
dBm	decibel milliwatts
DC	direct current
DE	diffusion equation
DLIA	digital lock-in amplifier
DPF	differential pathlength factor
DSP	digital signal processor
ECG	electrocardiography
EEG	electroencephalography
EMG	electromyography
EOG	electro-oculography
$ETCO_2$	end-tidal carbon dioxide
f_{-3dB}	-3 dB cutoff frequency
FD	frequency domain
fMRI	functional magnetic resonance imaging
FVU	fraction of variance unexplained
$[HbO_2]$	concentration of oxyhaemoglobin
[HbR]	concentration of deoxyhaemoglobin
HR	heart rate
HV	high voltage of photo-multiplier tube
IF	intermediate frequency

INA	instrumentation amplifier
iNO	inhaled nitric oxide
LO	local radio-frequency signal
LIA	lock-in amplifier
MEG	magnetoencephalography
MEMS	micro-electro-mechanical system
MT	movement time
NA	numerical aperture
NIR	near infrared
NIRS	near-infrared spectroscopy
NO	nitric oxide
NTC	negative temperature coefficient
N.U.	normalized unit
OP AMP	operational amplifier
PC	personal computer
PCB	printed circuit board
PD	photodiode
PH	pulmonary hypertension
PLL	phase lock loop
PMT	photomultiplier tube
R_{avg}	average reflectance
RC	resistor-capacitor
REM	rapid eye movement
RF	radio frequency
rms	root-mean-square
RVP	right ventricular pressure
S1−S4	sleep stages 1−4
SaO_2	arterial oxygen saturation
SDD	source-detector distance
sMSE	standardized mean squared error
SNR	signal-to-noise ratio
STD	standard deviation
TD	time domain
TMS	transcranial magnetic stimulation
TOI	tissue oxygenation index
totHb	total haemoglobin
TPSF	temporal point spread function
VCXO	voltage-controlled crystal oscillator
VEP	visually evoked potential
VLF	very-low frequency
VLFO	very-low-frequency oscillation

List of Symbols

α	extinction coefficient
ΔA	logarithmic change in light modulation amplitude
ϕ	phase shift
I_{AC}	modulation amplitude
I_{DC}	average intensity
λ_{i}	wavelength
μ_a	absorption coefficient
μ_s'	effective scattering coefficient
p	p-value of statistical test
p_1	p-value of paired statistical test
p_2	p-value of unpaired statistical test
R^2	coefficient of determination

1 Introduction

Medical near-infrared spectroscopy (NIRS) utilizes near-infrared (NIR) light (650 - 950 nm) to study the oxygenation and hemodynamics of tissue non-invasively [1]. In a typical setup, NIR light is delivered to tissue using optical fibers and detected a few centimeters from the point of illumination. Traditionally, NIRS has been applied to monitor local changes in the concentrations of oxy- ($[HbO_2]$) and deoxyhaemoglobin ([HbR]), which are the two strongest NIR light absorbers in most tissues [2]. These parameters are related to physiologically interesting phenomena such as changes in blood oxygenation and volume [1–5].

In addition to absorption, scattering affects on the propagation of NIR light in tissue. In fact, scattering is more than ten times more probable than absorption in typical tissues so that accurate quantification of $[HbO_2]$ and [HbR] becomes a challenging problem. By measuring the attenuation of light in tissue, relative changes in $[HbO_2]$ and [HbR] or the tissue oxygen saturation $\Big([HbO_2]/\big([HbO_2]+[HbR]\big)\Big)$ can be derived. Single and few-channel NIRS devices have already been used in clinical practice to monitor, e.g., brain oxygenation [6–9]. However, further improvements in quantification accuracy and measurement reliability are needed before NIRS is adopted in wide-scale as a routine cerebral monitoring method [10–12].

Scattering increases the mean pathlength of photons traversed through tissue. If both the mean pathlength and the attenuation of light are measured, the absorption and scattering properties of medium can be separated, which improves the quantification accuracy of NIRS [13]. Using the frequency-domain (FD) or the time-domain (TD) technique, a mean photon pathlength can be measured [13]. During the last 10 years the development of multichannel instruments has opened up possibilities for imaging applications as well [6, 14–17].

Multimodal monitoring and imaging is a rapidly growing area of research and clinical practice [18–22]. Different techniques provide somewhat different anatomical and physiological information with their benefits and limitations so that an integration of techniques usually provides more comprehensive data. Electroencephalography (EEG), for instance, measures mainly the electrical activity of neurons in the brain, but is not very sensitive to hemodynamic changes [23]. NIRS is, in contrast, currently the only technique providing a possibility for a bedside monitoring of brain oxygenation and hemodynamics with a sub-second temporal resolution. In many ways NIRS is an optimal method for multimodal measurements because light does not interact with the electromagnetic signals used in the other brain measurement methods.

Objectives of the thesis and an outline of the overview

In Sect. 2, the background of NIRS methods and techniques are briefly described. Publication I provides a detailed review especially emphasizing imaging approaches.

This thesis had three objectives. The first objective was to expand the existing FD instrument by increasing the number of detector and source channels and measurement wavelengths. In Sect. 3 of this overview, the author's contributions for implementing the FD instrument and multimodal techniques for NIRS studies are described. Other main objectives were to apply the FD instrument and NIRS methods to multimodal brain studies and to develop a novel method to detect a source coupling error in a forehead NIRS measurement.

Four different studies using our FD instrument and NIRS methods for human and newborn lamb brain measurements were carried out (see Sect. 4). The effects of instrumental parameters on the sensitivity to detect hemodynamic changes induced by breath holding and hyperventilation were tested. Changes in [HbO_2] and [HbR] during a natural sleep were also measured with our FD instrument. Relationships between the baseline blood flow and visually-evoked hemodynamic and neuronal responses in a multimodal NIRS-EEG setup were studied. Sect. 4 concludes with a multimodal monitoring study of newborn lamb, in which a commercial CW NIRS monitor was used.

The linearity of FD measurement parameters as a function of source-detector distance (SDD) detected on the human forehead is studied (see Sect. 5). Based on the loss of regression of phase data, a method was developed to detect an error in the coupling between a source fiber and tissue. The method is applied to investigate the effects of such coupling errors on the contrast, noise and depth sensitivity in a multichannel FD NIRS measurement. The discussion of the most important results and the closing remarks of this thesis are presented in Sect. 6.

2 Methodological and theoretical issues of NIRS

2.1 Tissue optics and physiology

Light absorption of water is rather low below 950 nm. However, approximately $70-80\%$ of tissues is water, so it has still some contribution to the NIR light absorption. On the other hand, light absorption of haemoglobin, especially [HbR], decreases at wavelengths above 650 nm. Therefore, using light at this wavelength range it is possible to detect signals through several centimeter thick tissues. Furthermore, HbO_2 and HbR have clearly different absorption spectra at NIR wavelengths making it possible to optically examine the oxygenation of blood and tissue [2,24,25]. Other oxygenation-dependent absorbers such as cytochrome oxidase (Cyto-Ox) have also been studied with NIRS but its contribution to NIRS signals is relatively small and more difficult to detect [26,27].

When a photon is absorbed in tissue, its energy is converted into thermal energy. This heating effect is rather low, even lower than the increase of tissue temperature due to sunlight during a sunny day [28]. In addition, NIR light does not have any ionizing effects so the technique is generally safe. This makes long-term and repeated measurements possible. Absorption in tissue is characterized using an absorption coefficient μ_a, which is a product of the concentration and the specific extinction coefficient α of the absorber. Because tissue consists of several absorbers, the total μ_a is a sum over μ_a of all individual absorbers.

The Beer-Lambert law states that in a non-scattering medium the attenuation of light A is directly proportional to the product of μ_a and the pathlength L of detected photons as

$$A = -ln\left(\frac{I}{I_0}\right) = \mu_a \cdot L, \tag{2.1}$$

where I_0 is an incident light and I detected light intensity. From this relationship, using measurements at several wavelengths the concentration changes of HbO_2 and HbR in tissue can be derived (see Subsect. 2.3).

Even though the most interesting physiological information in NIRS signals is related to the light absorption in haemoglobin, elastic scattering is a dominant process that affects the propagation of NIR light. Due to this diffuse nature, NIRS imaging is known as diffuse optical imaging [Publication I]. The scattering is characterised with an effective (or reduced or transport) scattering coefficient μ_s'. If the scattering is isotropic, the inverse of scattering coefficient represents the mean free path of a photon between two sequential scattering events. Also, scattering changes take

place in tissues [29,30]. However, they are assumed to be relatively small compared to absorption changes. Furthermore, the physiological interpretation of scattering changes is difficult. Differences in μ_s' can be observed, e.g., in imaging applications between different anatomical structures [31,32]. Fortunately the μ_s' and μ_a of skull are low enough to enable the investigation of cerebral tissue through the intact scalp.

Hemodynamic signals and their interpretation

Haemoglobin carries oxygen from lungs to peripheral tissues. When tissue is activated, the nutrient and oxygen consumption in cells is increased. The blood flow is therefore increased in the activated areas by several controlling pathways [33–36]. The coupling between cellular and hemodynamic mechanisms forms the base of functional studies with NIRS [3, 34, 37]. During a typical hemodynamic response, [HbO_2] increases and [HbR] decreases within a couple of seconds after the increase of cellular activity. When a stimulus or task is completed the [HbO_2] and [HbR] return close to their initial levels typically within 5-10 s [38]. With functional magnetic resonance imaging (fMRI) the blood oxygen level-dependent (BOLD) signal is measured, which reflects changes only in [HbR] [39–42]. Different areas of the brain are specialized to different kinds of cognitive processes and to control different body functions. Measurements at several locations make it possible to localize the brain areas which are mostly activated.

NIR light probes tissue volume that contains blood in arteries, veins and capillaries. Roughly two third of blood is in veins and most of the oxygen is extracted to tissue in capillaries. NIRS signal is assumed to be a weighted average of the [HbO_2] and [HbR] in all these three compartments [43, 44]. Furthermore, different vascular phenomena can create similar and often temporally overlapping changes in NIRS signals. An increase in blood volume increases both [HbO_2] and [HbR], whereas an increase in blood flow and a decrease in oxygen consumption increases [HbO_2] and decreases [HbR]. An increase in oxygen consumption creates opposite changes [45]. In addition, changes of blood flow and volume are coupled non-linearly [46, 47]. Therefore, the interpretation of NIRS signals is often challenging and may require additional knowledge or approximations on investigated physiological systems [48, Publication III, Publication V].

2.2 Measurement techniques and instruments

In the continuous wave (CW) measurement, the attenuation of light in tissue is measured. The first NIRS instruments as well as most of the current commercial

instruments are still based on the CW technology [1, 6, 49]. CW instruments are typically less expensive and less complex than FD or TD instruments. Using multichannel configurations, also quantitative values such as tissue oxygen saturation can be derived [7, 9, 50].

The TD method is the most advanced NIRS technique [15, 16]. In this method, pico-second long light pulses are emitted into tissue and the time-of-flight distribution of detected photons is measured, from which a temporal point spread function (TPSF) can be determined. The mean value of TPSF is directly proportional to the mean pathlength of photons and the area to the intensity of detected light [51–53]. The TD technique makes it also possible to select photons which have propagated through different depths in tissue by accepting photons only in a restricted time window [54, 55]. This procedure, however, decreases the overall signal-to-noise ratio (SNR) of TD measurement, because some of the detected photons are rejected. This can be compensated by increasing the measurement time. In general with the TD technique, the lowest light detection limit among all NIRS techniques can be achieved.

In the FD technique, light intensity-modulated at radio-frequency (> 50 MHz) is delivered into tissue. The average intensity (I_{DC}), the modulation amplitude (I_{AC}), and the phase shift (ϕ) with respect to the incident phase are measured [56,57]. The ϕ measurement is directly proportional to the mean pathlength of photons in tissue at frequencies < 200 MHz [58]. If I_{AC} and ϕ are measured at all the frequencies, the same information can be obtained with the FD and TD techniques [59, 60]. This approach, however, increases the complexity and measurement time of a FD instrument and may decrease its dynamic range and repeatability. In addition, only a single frequency measurement of I_{AC} and ϕ is needed to resolve the μ_a and μ_s' independently in an object [61]. This was one of the main reasons to select a single-frequency FD technique in our project.

The measurement instrument attenuates and produces temporal delays in the emitted and detected signals. When only relative changes in signals are measured, these instrumental responses are cancelled out provided that they are temporally constant [62]. However, if the absolute values are to be studied, the instrument has to be calibrated to remove the instrumental effects on the measurement variables [63]. Often, the calibration has been realized using a reference phantom with known optical properties and a geometry similar to that of the object under study [64–66]. In those cases the relative changes upon the known reference values are measured. In an other approach all instrumental responses are determined in independent calibration measurements and corrected so that the instrument can provide directly absolute quantities [67, Publication II]. In this thesis, we utilize our independent

calibration procedure to obtain absolute ϕ values from the human forehead.

A review by Chance *et al* reports the state-of-the-art of FD techniques of late 1990's and gives valuable advice and lists some challenges in the implementation of FD system [57]. A review by Wolf *et al* lists recently developed scientific and commercial NIRS instruments [6]. Some recent FD systems are designed for special applications such as for optical mammography [59, 68, 69] or for the imaging of finger joints [70]. In addition, several FD systems designed mainly for the monitoring of brain function have only a single channel [71–74] or few channels integrated in a special measurement probe [4]. Recently, a multi-frequency tomographic system based on a network analyzer has also been reported [60].

A recent comparison between our FD instrument [Publication II] and a state-of-the-art TD system [16] revealed some advantages of the FD measurement technique [75]. It provides I_{AC} and I_{DC} data with considerably better SNR and reproducibility with less expensive instrumentation than the TD technique. The I_{AC} and I_{DC} signals generally provide better contrast to hemodynamic changes than the ϕ signal [Publication III]. The FD technique then gives the same physiological information as the TD technique in shorter measurement time, which is a clear benefit in several activation and monitoring studies [76–79].

In Publication I the measurement principles, the basic structures of instruments, the detector and source techniques and calibration procedures of all three NIRS methods are summarized in more detail.

2.3 Modeling of NIRS signals

Typical NIRS models, such as the modified Beer-Lambert law, neglect temporal variations in scattering in which case light attenuation changes are only due to changes in absorption [25, 51, 80, 81]. This model also assumes a homogeneous tissue and that the absorption changes occur uniformly in a probed volume, which may not be true in most of physiological measurements [82].

Typically, at least two measurement wavelengths are used in NIRS. In addition, all the absorption changes are often assumed to be caused by the changes in [HbO_2] and [HbR]. Using the above mentioned simplifications, the relative changes in signals can be solved with the modified Beer-Lambert law as [25],

$$\begin{bmatrix} \Delta[HbO_2] \\ \Delta[HbR] \end{bmatrix} = (\alpha^T\alpha)^{-1}\alpha^T \begin{pmatrix} \frac{\Delta \mathbf{A}_{\lambda_1}}{SDD \cdot DPF_{\lambda_1}} \\ \frac{\Delta \mathbf{A}_{\lambda_2}}{SDD \cdot DPF_{\lambda_2}} \\ \vdots \end{pmatrix} , \tag{2.2}$$

where $\Delta\mathbf{A}_{\lambda_\mathrm{i}}$ is the logarithmic change in I_{DC} or I_{AC} at wavelength λ_i with respect to some arbitrary baseline, DPF is the differential pathlength factor, and α a $2 \times \mathrm{M}$ matrix containing the specific extinction coefficients of absorbers at different wavelengths [2]. In all studies of this work, the extinction coefficients were taken from [2]. The mean pathlength of photons in tissue can be written as $SDD \cdot DPF$. The objectives of the thesis were mostly on instrument and methodological development, so that this simple but widely used model was utilized in the brain studies.

Beyond the modified Beer-Lambert law, more advanced approaches have been developed to model the light propagation in tissue and to derive quantitative values for physiological parameters. The most common light propagation model in diffuse optical imaging is the diffusion equation (DE). In some simple geometries DE can be solved even analytically [58,83,84]. Based on such analytical solutions, spatially-resolved techniques utilizing measurements at several SDDs have been employed to solve the ratio of μ_a and μ_s' [50]. With the frequency- or time-resolved techniques utilizing also the pathlength measurement, the absolute values of μ_a and μ_s' can be derived [83, 85, 86]. With some further approximations, absolute values of [HbO_2] and [HbR] can be determined from μ_a [4, 87, 88]. In optical topographic imaging, two-dimensional maps, typically without depth information, are straightforwardly interpolated [89]. These techniques, however, suffer from, e.g., partial volume effects [82]. If an object contains layers with distinguishable optical properties, multilayer models can be applied [90–92]. To resolve continuous distributions quantitatively, optical tomographic imaging techniques are required [93]. Light propagation models and image reconstruction approaches in diffuse optical tomography are reviewed in more detail in Publication I. Our FD instrument has been shown to provide appropriate data also for three-dimensional absolute tomographic imaging [Publication II].

2.4 Couplings between multimodal measurement parameters

Changes in heart rate (HR) typically increase the cardiac output, which may lead to an increase in cerebral blood flow and volume [48, Pulication III]. These flow changes can be detected, e.g., using Doppler ultrasound measurement on the carotid artery [94, Publication V]. If the arterial oxygen saturation (SaO_2) decreases, it can also decrease the total cerebral tissue oxygen saturation [95]. This thesis will show that changes in these systemic circulatory parameters can induce changes in NIRS signals [Publication III]. On the other hand, NIRS makes it possible to directly monitor hemodynamic and oxygenation changes from the cerebral tissue which are not necessarily coupled to systemic circulation parameters [Publication V]. If EEG is used to monitor the sleep stages with a simultaneous cerebral NIRS

measurement, the hemodynamic changes related to the level of consciousness can be studied [96–98, Publication III]. Also, if baseline blood flow is changed during simultaneous NIRS-EEG measurements of stimulus-evoked responses, links between these neuronal and hemodynamic processes can be investigated.

In addition to cerebral studies, NIRS has been applied extensively to study the function of skeletal muscles and to optical mammography [Publication I].

3 Instrumentation

When this work started, a single source- and detection-channel and a single wavelength FD instrument had been developed [74]. The goal of our group was to implement a multichannel instrument capable of measuring the mean photon pathlength with good accuracy and simultaneously providing as good SNR as possible to detect physiological signals in tissue with a sub-second temporal resolution.

The FD instrument was extended first from 1 to 16 time-multiplexed source channels and to 4 [99] and afterwards to 16 parallel detection channels [Publication II]. The second measurement wavelength was included to enable spectroscopic studies [Publication II] and afterwards four laser diodes were integrated in the system [100]. The original articles of this thesis do not include the detailed descriptions of any implemented parts of FD system or other instrumentation reported in Subsects. 3.2−3.7.

3.1 Operation of the frequency-domain imaging instrument

The structure of the current version of our FD instrument is shown in Fig. 3.1. The instrument has been designed and implemented in the Laboratory of Biomedical Engineering (at present the Department of Biomedical Engineering and Computational Science) at the Helsinki University of Technology mainly by four group members. During 2002 it was moved to the BioMag Laboratory located at the Helsinki University Central Hospital to enable its performance testing in neonatal and adult brain measurements.

The instrument includes four temperature-stabilized laser diodes modulated at 100-MHz frequency. The diodes are biased with current sources and modulated with a general-purpose signal generator. The RF shielded package including the diode, a reactive matching circuit, and a negative-temperature-coefficient (NTC) resistor is surrounded with peltier-elements and heat-sinks. The peltier-elements and NTC resistors are part of the temperature-stabilizing system of the laser diode (Subsect. 3.4.2).

A 4×1 fiber-optic micro-electro-mechanical-system (MEMS) switch (Subsect. 3.4.1) is used to select a single source wavelength and a 1×16 MEMS switch a single source position active at a time. Light is delivered to the surface of an object through a 100-μm optical fiber and collected using fiber bundles with a 2.5-mm active diameter. The light signal is detected using 16 parallel photo-multiplier tubes (PMT) encased in the modules (H6780-20, Hamamatsu Photonics, Japan).

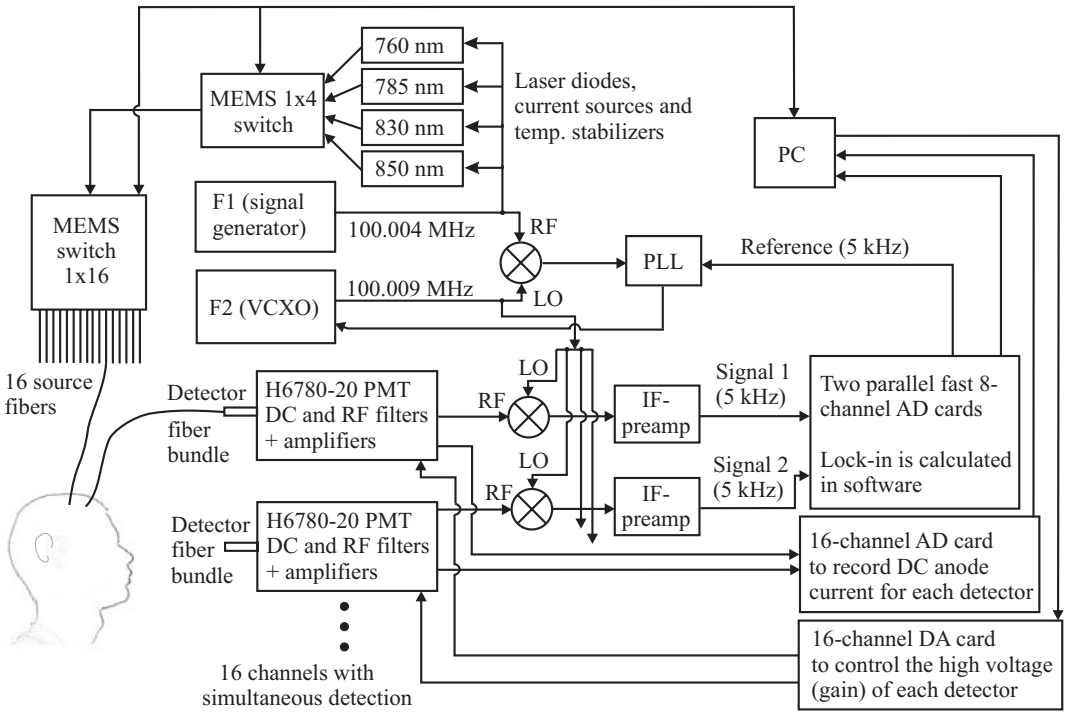

Figure 3.1: Block diagram of the current structure of the FD instrument.

The measured signal (RF) is amplified in two stages and mixed with a local radio-frequency signal (LO) to produce a 5-kHz signal. The LO signal is generated by a voltage-controlled crystal oscillator (VCXO) and divided by two power splitters. The mixer output is low-pass filtered ($f_{-3dB} \sim 1$ MHz) and guided into an intermediate frequency (IF) amplifier (see Subsect. 3.2), which is the preamplifier for an analog-to-digital (A/D) converter. The signals are sampled with two parallel 8-channel data acquisition cards using a 20-kHz sampling frequency.

The heterodyne measurement technique with a phase-lock loop (PLL) and a digital lock-in amplifier (DLIA) with a 5-kHz reference signal ensure a high measurement accuracy [74, 99]. The PLL feedback loop consists of the VCXO, a phase detector and a low-pass filter. The PLL circuit is controlled by a reference signal from the DLIA and a signal from another mixer. From these two signals, the PLL circuit with a low-pass filter in its output generates a control voltage for the VCXO. The PLL adjusts the frequency difference between the VCXO and the signal generator (F1) to be the same as the reference frequency. Then the phases of the measurement and the DLIA reference signals become synchronized. After a measurement, the I_{AC} and ϕ difference of the sampled IF signals with respect to the reference signal are calculated in PC using a DLIA algorithm. In the heterodyne technique, the I_{AC} and ϕ of detected RF signal are directly proportional to those of the measured IF signal.

The anode current is also low-pass filtered and amplified. This signal measured using a data acquisition card is directly proportional to the I_{DC} of detected light. The PMT high voltages (HV) are adjusted using an analog output board (National Instruments, PCI-6704). If too high an anode current is used, an intra-channel phase-amplitude crosstalk is generated inside the PMT. The anode current can be controlled by changing the HV (or gain) of PMT. A crosstalk can be eliminated, if the anode current is kept below 70 nA [Publication II]. Therefore a prescan is carried out before each measurement to adjust optimal HV values for each source-wavelength-PMT combination. This way the gain is maximized in PMTs without causing crosstalk. This implementation makes it possible to measure phase and amplitude independently with a high dynamic range (approximately 1:10^6) and low noise floor.

3.2 Design and implementation of preamplifiers

16 parallel IF preamplifiers were designed and implemented [100]. The preamplifiers should amplify the 5-kHz IF signals $\sim$ 65 - 105 dB and filter the out-of-band noise before A/D conversion. To improve the SNR, the noise level of each sequential amplification stage has to be lower than that of a preceding stage. The amplifiers should not have a detectable inter-channel crosstalk either.

The preamplifiers are placed in two identical aluminium cases each containing eight preamplifiers. The preceding mixers are shielded in a separate case. The cases provide relatively stable but somewhat different ground potentials for those circuits. A proper decoupling was required to minimize possible ground loops between the sequential electronics. The input of A/D converter board included a multiplexer with a 100 pF capacitance between adjacent channels. No capacitive components were included in the output of the amplifier circuit because additional capacitance would increase the discharge time of multiplexer producing unnecessary crosstalk between the adjacent A/D converter channels.

The final implementation includes three sequential operational amplifiers (OP AMP) in a non-inverting configuration. The filtering is realized with 2nd-order resistor-capacitor (RC) band-pass filters between sequential amplification stages (see Fig. 3.2). A precision OP AMP (Analog Devices, OP27) with a low noise ($3\text{nV}/\sqrt{\text{Hz}}$) and input offset voltage ($\sim$ 30 μV), high common-mode rejection ratio of $\sim$ 120 dB and relatively large gain-bandwidth production (8 MHz) was selected.

Resistances in a kΩ range were used to reduce the leakage currents from the signal paths to the ground. The first two amplifier stages have a fixed amplification (+34.3 dB) and the third is manually adjustable between 0 and +40.6 dB. A pseudo-

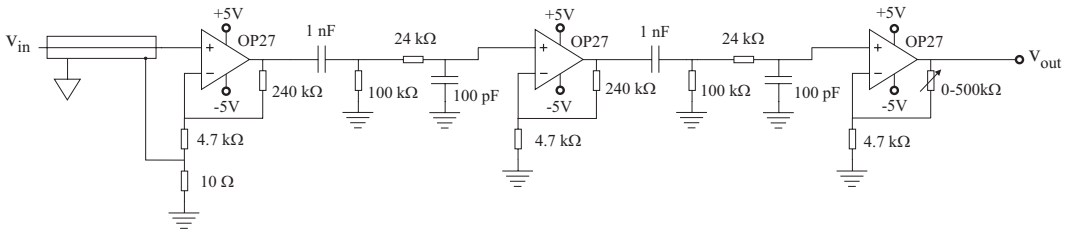

Figure 3.2: The block diagram of the final layout of preamplifier.

differential input stage was used to disconnect ground loops between the cases. This was implemented by grounding the first amplifier through an additional 10 Ω resistor. The ground voltage of the mixer case was isolated from the preamplifier case and connected directly to the other end of the 10 Ω resistor. The first OP AMP then amplifies the voltage difference between the signal and the ground of the mixer case.

A two-layer printed circuit board (PCB) was designed using the PowerPCB program (Mentor Graphics). The electronics were assembled using the Philips ACM Micro assembly machine in the Laboratory of Electronics Production Technology at the Helsinki University of Technology.

3.2.1 Noise and crosstalk measurements

The output noise and interchannel crosstalk were measured to evaluate the performance of preamplifiers. The noise measurements were carried out in two cases: the RF amplifiers following the PMTs were turned off and on. The amplifications were set between $+80 - 87$ dB, which corresponds to normal operation of preamplifiers. When the RF amplifier is off the positive input of preamplifier is grounded through the 50 Ω resistors inside the preceding mixers to the ground of mixer case. The noise of preamplifiers would have been ~ 5 – 10% lower if the positive inputs of preamplifiers were directly short-circuited to their own ground potential. When the RF amplifiers were switched on their output noise was added to the measured signals. When the PMTs were switched on with zero HVs no increase in noise of the RF amplifiers outputs were observed so the PMTs were switched off in all measurements.

The noise levels were measured using a digital oscilloscope (LeCroy, Waverunner). The standard deviation (STD) of signals was measured five times. When the RF amplifiers were turned off, the range of mean noise levels was $24.4 - 50.6$ mV and when turned on it was $236.7 - 108.7$ mV. This means that the preamplifier noise level is ~ 4 to 5 times lower than the output noise of the RF amplifiers.

To reveal possible interchannel crosstalk, the 5-kHz signal with an effective amplitude of 40 mV from a generator (HP-33120A, Hewlett-Packard) was fed into a preamplifier while the other preamplifiers were connected to the preceding mixers. The measurement signal was attenuated with three sequential -20 dB attenuators (SAT-20, Mini-Circuits). A SR810 DLIA (Stanford Research Systems) with a 1-s time constant and a maximum sensitivity setting could not detect any interchannel crosstalk. In a typical measurement, the effective amplitude of the active channel is 3.2 V and the noise level of these measurements overwhelming the crosstalk was $\sim$ 0.04 mV. Therefore the crosstalk has to be at least 98.1 dB lower than the active channel signal.

3.3 Digital lock-in amplifier

During the development of the FD instrument, a four-channel DLIA based on the digital signal processor (DSP) technology was developed [99]. A four-channel A/D converter board was designed to extend a commercial DSP evaluation board (ADSP-21065L EZ-LAB, Analog Devices). The A/D converter board includes approximately 150 components and 800 connection pads. The noise level of the final implementation is -86 dB whereas the maximum reachable noise floor of the designed system would have been $\sim$ -88 dB. A LIA program was written using an assembly language of DSP (ADSP-21065L SHARC, Analog Devices). The necessary electronics were designed to integrate the DLIA with the FD instrument and it was used as a part of the instrument during a four-channel configuration.

3.4 A four-wavelength source system

NIRS applications generally utilize at least two wavelengths. Our first source system contained two 5-mW laser diodes with temperature stabilizers, current sources, and a 1×2 prism and 1×16 moving-fiber switch (DiCon Fiberoptics, Inc.) to select the active wavelength and source position [Publication II]. During this work the controlling software and connection electronics were implemented to enable the wavelength and source multiplexing [99].

The two-wavelength system required improvements. The $\sim$ 20-Hz maximum switching frequency for wavelength data needed to be increased to make it possible to measure blood pulsation signals with a better temporal accuracy [48, 101, Publication III]. The 1×16 source switch was also slow (switching time $>$ 300 ms) making it impractical for most physiological applications. The 1×2 prism switch produced a disturbing switching sound. PCBs of the temperature stabilizers were unnecessarily large including some grounding and stability problems and required two

external voltage sources. A higher laser power than $\sim$ 5 mW was desired for most applications improving SNR. Some applications also benefit from more than two wavelengths [Publication I] leading to the design of a new four-wavelength source system [100].

3.4.1 Wavelength and source switches

A source switch was desired consisting of at least 16 channels with a maximum switching time of $\sim$ 10 ms. The inter-channel crosstalk was required to be $\leq$ -80 dB, the switch should have low losses and should not add noise to the measured signals. In addition, the switch should be silent because the instrument was aimed to be used in auditory activation studies. Possible solutions compared included an own implementation, e.g., based on an optical coupler and camera shutters or a fast servo motor and a rotating small mirror [17], mechanical moving fibers or prisms, liquid crystal, acousto-optics, electro-optics, magneto-optics, and piezo switches. A switch based on the MEMS technology provided the best combination of the required features although its inter-channel isolation was only moderate [100]. Because the isolation was not a critical parameter in wavelength switching, a 1×4 MEMS switch (Opneti Communications Co) was purchased for that purpose and for testing. To control the switch a code using the two data bits from a PC parallel port was written.

The influence of 1×4 MEMS switch to the short-term repeatability of the FD instrument was tested. The amplitude and phase data were recorded from a homogeneous polyester resin phantom having optical properties similar to those of living tissue. In all measurements, the wavelengths of 760 and 830 nm with the highest optical powers available (6.4 and 8.4 mW) and a single channel with a $\sim$ 2-cm SDD were used. An HV of 275 V was set to the PMT, resulting in an anode current close to 70 nA. The first $\sim$ 60 s of reference data were measured at both wavelengths without switching. Then the signals were measured while switching the two wavelengths at 10-ms and 100-ms intervals. Finally, all four channels were switched at 100-ms intervals. The results indicated that the MEMS switch did not induce any detectable noise into the signals.

The inter-channel isolation of the switch was also studied. In those measurements, light from the 785-nm laser was coupled to one of the output fibers of the switch and passive channels were measured using the FD instrument. The light attenuation in the measurement setup was determined separately using an optical power meter (Thorlabs, Model S20MM). The isolation was derived as the ratio of the optical power in the passive channel to that in the active channel, where the attenuation of the measurement setup was taken into account. The optical power in the passive channel was determined from the average value of anode current, the HV, and the

sensitivity factor of the PMT. The highest crosstalk of -65.0 – -65.2 dB was detected from channel 4 to channel 1 in two separate measurements. Otherwise the level of crosstalk varied between -76.0 – -110.0 dB having mean ± STD = -83.0 ± 13.9 dB. Afterwards, a 1×17 MEMS switch (Opneti Communications Co) including 16 active and 1 off channel was integrated into the new source system [102].

3.4.2 Laser diodes, their current sources and temperature stabilizers

Two 100-mA current supplies were implemented to bias the laser diodes so that their modulation with a RF signal becomes possible. The operation of the supplies is based on the feedback loop of an ultra-low noise OP AMP (LT1028, Linear Technology) which is connected to an n-channel MOS transistor (VN0300L, Siliconix Incorporated) [103]. The advantages of such supplies include low noise and good temperature stability.

To ensure intensity and wavelength stability the laser diodes must be temperature stabilized. The design of the stabilizing electronics is based on its previous implementation (Fig. 3.3) [74]. The goal was to accomplish a more compact PCB with improved performances than previously. The implemented stabilizer cir-

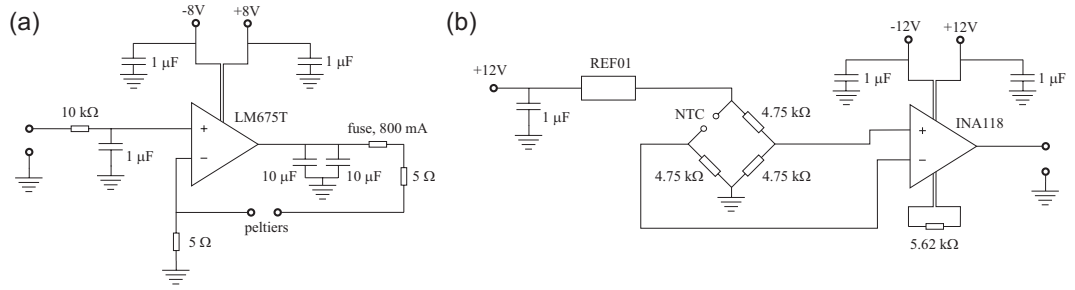

Figure 3.3: Block diagrams of a) adjustment and b) measurement section of the temperature stabilizers implemented in this work.

cuit consisted of separate sections for adjusting and measuring temperatures. The power OP AMP (LM675T, National Semiconductor) of the adjustment loop forms a simple current supply. It provided a control current for four peltier elements (MI1010T, Marlow Industries) connected in series in the RF shielded housing of the laser diodes. The temperature changes inside the housing were detected with a NTC resistor (GM472W, Thermometrics) in a bridge connection of equal value resistors. The voltage differences across the bridge were amplified with instrumentation amplifier (INA118P, Texas Instruments) and sampled with a data acquisition board. The control current level was adjusted with a digital feedback algorithm through the data acquisition boards [104].

The adjustment loop of the previous implementation was not stable across the whole control voltage range. The circuit was redesigned to operate stably providing as much output current to the load as possible. The return paths of the power OP AMP were designed, the resistances were reselected, and smoothing capacitors were added in the peltier adjustment loop. In the new design a single ±15 V power terminal with a ground connection was delivered to the PCB. The different supply voltages for the measurement and adjustment sections were regulated inside the board. A special effort was made to isolate the supply voltages between the sections and to stabilize them inside the sections. In addition, a particular emphasis in the design of the PCB was given to the grounding and the placement of components. The possibility that a ground noise from the adjustment loop could couple to the measurement section was to be minimized. The size of the new PCB is about one fourth of that of the previous one while it contains twice as many components.

The noise level of the stabilizer circuits was determined by measuring the root-mean square (rms) of the INA output voltage with respect to the ground with an oscilloscope (9361C, LeCroy). For these measurements the NTC resistors were replaced with 4.7-kΩ low-noise metal-film resistors. The noise levels of all four stabilizer boards were between 0.36 - 0.39 mV_{rms}, which is close to the theoretical input noise level of the A/D converter boards ($\sim$ 0.22 mV_{rms}).

Possible crosstalk between adjustment and measurement sections were determined as well. Instead of the NTCs, the same 4.7-kΩ resistors were used here as well. The adjustment circuits were sequentially run using a 1-kHz control voltage from a signal generator (HP-33120A, Hewlett-Packard). Signals above 1 kHz are efficiently attenuated in the input filter of the adjustment loop so that they were not analysed. A control signal close to a saturation level was used. The power spectra from the outputs of the INAs at 1 kHz as well as the background noise levels were measured with the oscilloscope. When the replacement resistor was attached directly to the terminal block of the temperature-measurement circuit, the magnitude of crosstalk was between -75.5 and -80.6 dBm and the background noise level was between -85.0 and -87.4 dBm. When the resistors were fixed to the terminal blocks of the laser housings, the crosstalk signal increased to between -51.8 and -55.5 dBm. This additional crosstalk due to the signal cables from the NTC resistors to the measurement circuits was further investigated. The measurements were repeated at the lowest possible control frequency of 100 Hz from the signal generator indicating an insignificant crosstalk being between -76.2 and -81.6 dBm when the cables were properly shielded. The normal maximum control frequencies used are < 10 Hz in which case the crosstalk would be undetectable.

Four laser diodes at wavelengths 760, 785, 830, and 850 nm and with the output

powers of 20, 55, 40, and 60 mW respectively were selected for the new source system [100]. Two wavelengths are HbO_2-sensitive and two HbR-sensitive. Longer wavelengths were not considered because the sensitivity of the cathode material of our PMTs strongly decreases with increasing wavelength. On the other hand, high-power ($\geq$ 20 mW) laser diodes at wavelengths below 760 nm were not found at a reasonable price. The outputs of the laser diodes were coupled with an efficiency of 80 – 85% to the MEMS switch using commercial translators and collimation and focusing optics (Thorlabs, Inc.). As a final tuning, the output powers (12.6 – 17.5 mW), the DC currents, and the RF powers were balanced between the laser diodes, the final modulation depths being between 72 - 87 %. The output powers of the diodes were maximized and balanced so that none of them exceeded 20 mW, which is still considered safe for lasers in research use [28].

3.4.3 Encasing the system

The new source system was encased in a standard 3U rack case (see Fig. 3.4). The

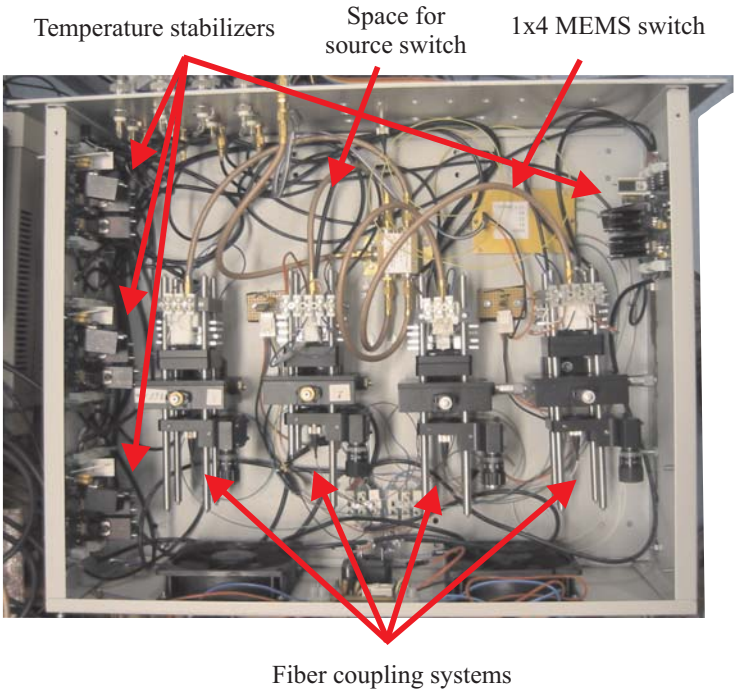

Figure 3.4: Photograph of the four-wavelength source system. Space in the front section of the case was reserved for a source switch.

four stabilizer circuits were fixed on the sides of the case enabling a proper grounding and relatively easy access to all terminal blocks of the boards. Four fiber-coupling systems with the laser diode housings were located in a row in the middle of the case so that the lasers can be collimated in their final places. The supply voltages

were delivered through a single three terminal ±15-V connector and regulated when needed for the different components inside the case. The wavelength switch was located in the front section of the case.

3.5 Arranging the instrument into a cabinet

For measurements outside the laboratory it was necessary that the system be portable (see Fig. 3.5). This was important also for the start of multimodal studies.

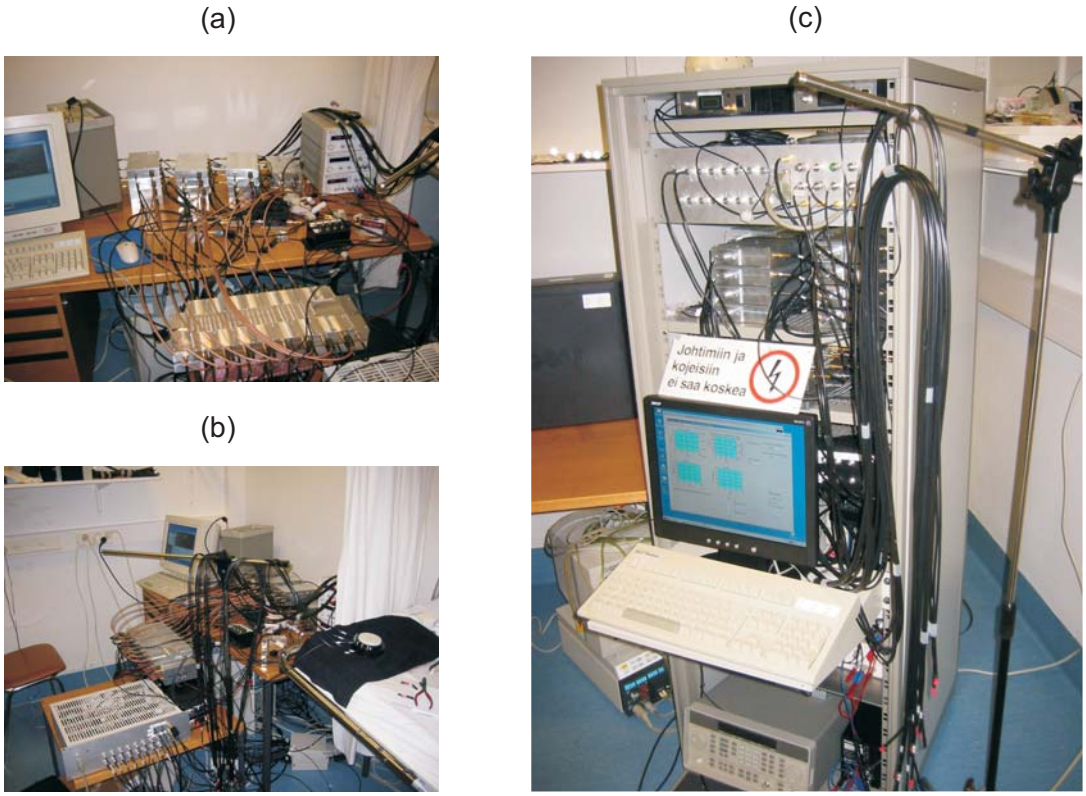

Figure 3.5: The FD instrument a) and b) before and c) after the modification.

The different parts were arranged in a standard 19 inch Eurorack cabinet at the beginning of year 2005. A centralized power supply system was realized by replacing laboratory power supplies with high quality DC supplies with a Eurocard rack mounting (Delta Elektronika BV 75 SX 15-15). Attempts were made to retain the relatively easy serviceability of different parts of the instrument. After the modification the short-term repeatability of the instrument [Publication II, Fig. 5] was verified to remain unchanged.

3.6 Detector and source fibers for multimodal brain studies

A technique enabling the integration of the FD instrument with transcranial magnetic stimulation (TMS), magnetoencephalography (MEG) or MRI was to be developed. MEG and fMRI measurements are generally carried out in a magnetically shielded room. Improperly shielded magnetic components inside a magnetically shielded room may break a MEG instrument or cause safety risks in MRI [105]. In contrast, TMS stimulation coil produces a relatively high magnetic field ($\sim$ 2 T) so that magnetic materials cannot be attached to the surface of the subject's head [106]. NIRS measurements simultaneously with MEG, fMRI or TMS are possible provided that completely nonmagnetic NIRS terminals are used inside a magnetically shielded room or with TMS. In addition, NIRS terminals on the subject's head have to be fitted inside a MEG helmet, MRI head coil or under TMS coil. Thus the terminals have to be small in size and preferentially attached tangentially to the head surface.

For such multimodal studies, 16 ten-meter long detector fiber bundles and 3 source fibers were purchased (Z-Light, Latvia). The active diameter of bundles is 2.5 mm. They contain approximately 300 multimode fibers with a 100-μm core and 110-μm cladding diameter (e.g., Optran UV 100/110P fibers). The numerical aperture of fibers is 0.22 and the bundle packing density is $\sim$ 75 %. The protective jacket was made from a flexible shrinkable black plastic. One end of the bundle is centralized in a 35-mm long cylindrical terminal with a 5-mm diameter (Fig. 3.6). The source fibers include the same fiber material as the detector bundles.

Figure 3.6: a) Photograph of prism (circled) and cylindrical terminals of fibers. b) Close-up picture of the prism terminal with one of the faces pointing upwards.

The other end of the source fiber and the detector bundle contains a terminal with a right angle micro prism (Lambda Research Optics, Inc.). The prism with 5-mm faces makes it possible to attach the detector and source terminals tangentially to an object surface. Both faces of the prism are covered with a multi-layer broadband

anti-reflection coating with an average reflectance (R_{avg}) < 0.5% between 650 and 950 nm at 0 °. The reflecting face is covered with silver (R_{avg} > 80% between 650 and 950 nm at 0 °) to maximize the reflection and with the black sealing paint. The height of the prism terminals is 5 mm, width 8 mm and length 18 mm. Both terminals were made of a black Ertacetal C which is hard, stiff and nonmagnetic engineering plastic enabling precise machining.

The compatibility of new prism terminals was tested with TMS. No movement of terminals was detected by eye when the terminal was located in the middle of a figure-of-eight stimulation coil (Magstim 200, Magstim Co) while applying pulses with a maximum intensity. TMS stimulation was, however, observed to magnetize the terminal. Therefore, the terminal induced relatively large artifacts when it was slowly swung close to the MEG detectors. The induced artifacts were reduced after a careful demagnetization of the terminals. The magnetization was most likely caused by the Epoxy used to glue the prism on the terminal [107]. In the next generation terminals, non-magnetic glue should be used.

3.7 Other instrumentation

Techniques for hyper- and hypocapnia studies

A breathing system was constructed to induce cerebral blood flow (CBF) changes by varying the carbon-dioxide (CO_2) content of inhaled and exhaled air. This was possible because CO_2 is a major regulator of CBF in the human brain [108]. The system consists of a gas bottle with a mixture of oxygen (21 %), CO_2 (8 %), and nitrogen (71 %), a manually adjustable rotameter to control the gas flow, a breathing mask with tubing to deliver the gas, and connectors to the gas module [100]. In the hypercapnia measurements of Publication IV, the hypercapnia was induced using gas-flow level of 6.0±1.0 l/min. In Publication VI, two different flow levels (1.8±0.3 and 7.2±0.4 l/min) were used.

An AS/3 patient monitoring system (Instrumentarium, Finland) was used. It contains a gas module to measure gas exchange parameters such as a capnogram with an end-tidal CO_2 ($ETCO_2$) and a spirometer to measure additional respiratory parameters. A hemodynamic module measures the HR using three electrocardiography (ECG) electrodes in the shoulders and in the left hip. It also includes a finger-attached pulse oximeter to measure SaO_2. For data transfer, a S/5 Collect software (Instrumentarium, Finland) having the capability to transfer about 150 trend parameters or digitized signal waveforms to PC was used. For these measurements, the most important reference parameters were $ETCO_2$, HR, and SaO_2 [100].

In Publication III a standard capnogram monitor (Normocap 200, Datex, Finland) was used to continuously monitor the CO_2 content of expiratory air.

Sleep-monitoring system

A standard sleep measurement facility was set up for natural sleep studies ([Publication III] and Subsect. 4.2). Polysomnography was used to record electrical activity and the sleep stages of the subject. The data were recorded using an ambulatory device (Embla, Flaga hf. Medical Devices, Iceland) containing a four-channel EEG (C4-A1, O2-A1, C3-A2, and O1-A2), a single-channel electromyography (EMG) for measuring muscle activity on the jaw, and a single-channel electro-oculography (EOG) for detecting eye movements. A single-channel ECG (electrodes on right and left arm) measures the HR and a pulse oximeter, attached to the subject's index finger, measures the SaO_2. A codec (DivX 5.1, DivX, Inc.) was used to capture video images from a standard monitoring camera into the PC to register subject's head movements.

Movement sensor

Motion artifacts are often harmful and set limitations for all medical imaging modalities [109–111]. Even though NIRS is not the most vulnerable method for the motion artifacts, they can still seriously complicate the acquisition of NIRS data as well [112, 113]. To avoid such problems, a two-axis inclinometer chip (SCA100T, VTI Technologies Oy, Finland) was included in our NIRS measurement setup to detect the subject's head movements [Publication IV]. First a laboratory-made solution was applied. A similar prototype detector was also developed by GE Healthcare Finland partly in parallel with us. Afterwards, this GE's sensor has also been used in our measurement setup.

NIRO-300 oxygenation monitor

A NIRO 300 (Hamamatsu Photonics K.K., Japan) NIRS monitor was applied to study newborn lambs ([Publication V] and Subsect. 4.4). These measurements were carried out in Lund University in Sweden. The NIRO 300 is an easily portable bedside monitor consisting of display ($\sim 390 \times 250 \times 340$ mm) and measurement ($\sim 140 \times 255 \times 85$ mm) units with some cabling. It uses four sequentially pulsed laser diodes (775, 813, 853, and 910 nm) as light sources. Our version of the instrument has a single channel. Light is delivered to tissue using an optical fiber

and detected using 3 parallelly integrated photodiodes (PD) which can be attached directly to the tissue surface using a probe holder and double-sided adhesive tape. The measurement probe provides either a 4- or a 5-cm measurement distance.

The monitor measures the changes in $[HbO_2]$, [HbR], total hemoglobin $\big([\text{totHb}] = [HbO_2] + [\text{HbR}]\big)$, and the redox-state changes of Cyto-Ox simultaneously with the tissue oxygenation index (TOI). The TOI is a ratio of $[HbO_2]$ and [totHb] given as a percentage in analogy with SaO_2. However, TOI indicates mostly venous blood oxygen saturation instead of that due to arterial blood [7, 43]

The concentration changes are calculated in NIRO 300 using the modified Beer-Lambert law (Eq. 2.2). To determine quantitative changes, a constant value for the differential pathlength factor (DPF) was taken from the literature. The TOI value is calculated in the monitor using spatially resolved spectroscopy [50]. The attenuation of intensity signals at the three PDs as a function of distance from the source is utilized. The derivation of TOI starts from a solution of diffuse reflectance in a homogeneous scattering medium in a half-space geometry [114]. With a few approximations and using an experimentally derived model for the wavelength dependency of tissue scattering coefficient, the ratio of $[HbO_2]$ and [HbR] can be derived [50, 115, 116].

4 Frequency-domain and multimodal brain studies

This section concentrates on the methods and findings of Publications III − V.

4.1 Hyperventilation and breath-holding study

This study summarizes the first human brain monitoring measurements with our FD instrument. Breath-holding and hyperventilation tasks were considered relatively easy and safe ways to induce hemodynamic and oxygenation changes in the brain. The principal purpose of the series was to test the sensitivity of the instrument to detect hemodynamic changes in the human head. Furthermore, the effects of SDD and measurement wavelength on the I_{AC} and ϕ signal contrast as well as the frequency content of the I_{AC} signals were investigated [Publication III].

Eight measurements were carried out on two subjects. The FD instrument at that time contained only a single laser source and four detection channels. Three measurements at 760 and 808 nm and two at 830 nm were carried out at the laser power of approximately 4 mW. The laser source was manually changed between the measurements. The I_{AC} and ϕ data were recorded during a sequence containing periods of rest (2 min), hyperventilation (2 min), rest (2 min), breath holding (2 min), and rest (2 min). The sequence was repeated once and the last rest period was 4 min resulting in a total measurement time of 22 min. The source fiber and the four detection bundles were attached to the left side of subject's forehead close to the hairline corresponding to SDDs of 2, 3, 4, and 5 cm. The fiber holder made of thermoplastic was individually shaped for each subject before measurements.

4.1.1 Results

In these measurements, better contrast-to-noise ratio (CNR) was found from I_{AC} than from ϕ data. The physiological interpretation of I_{AC} signals is also more straightforward so that they were selected for further analyses. It was further noticed that both contrast and noise content increased with the SDD [Publication III, Figs. 4 and 5]. The different measurement wavelengths were found to reflect different physiological phenomena. The decrease in CBF during hyperventilation tends to decrease the [HbO_2], which was detectable at the HbO_2-sensitive wavelength of 830 nm. Breath holding increases cerebral blood volume (CBV) and induces hypoxia which increases [HbR]. This effect was clearly detected at the HbR-sensitive wavelength of 760 nm [Publication III, Fig. 6]. The 2-min breath holding induced a nearly 50% decrease in these 760-nm signals at the SDD of 5 cm.

The frequency content of the amplitude signals was investigated with the power spectra. The time variations of the frequency components were analysed with spectrograms. Two dominant frequency components were found in each measurement. One component at 1 Hz was induced by the blood pulsation, especially in arterial compartments. Another strong component was found at very-low frequencies (VLF, 0.01 – 0.03 Hz). The physiological background of these oscillations is still somewhat controversial even though their existence has been verified by other measurement techniques as well [117, 118]. One possible explanation is circulatory autoregulation where small arteries fluctuate rhythmically causing slow vasomotions [119]. Our results support this theory because the VLF oscillations (VLFO) were clearer at HbO_2- than at HbR-sensitive wavelengths.

4.2 Natural sleep study

In modern countries, sleep disorders have become a common problem which affects the quality of life of an increasing number of people. Typical clinical techniques to quantify sleep and its disorders are personal interviews, questionnaires based on the patient's own observations, video or actigraphy recordings and bioelectrical measurements such as EEG [120–124]. Actigraphy measures the patient's movements and EEG the changes in electrical activity in the human brain. Polysomnography is a widely used multimodal sleep research technique, which consists of EEG, EOG, and EMG [120, 121]. Often also ECG and a pulse-oximeter are included to record global circulatory parameters such as changes in HR and SaO_2. However, a method to directly monitor local hemodynamic changes in the brain is missing from the clinically used sleep research techniques.

During natural sleep, various physiologically and neurologically interesting processes change the electrical activity of the brain [125]. It has been shown that natural sleep affects CBF and the cerebral metabolic rate of oxygen ($CMRO_2$) [126]. In disorders like sleep apnea, decrease in cerebral oxygenation and CBF may even lead to life-threatening consequences [120].

The interest of our research group towards multimodal monitoring, especially during anaesthesia and intensive care, was a main motivation for these natural sleep studies. Combined NIRS and EEG sleep studies could be carried out in a normal laboratory environment and they can provide a useful information for further monitoring studies. In fact it turned out that the detection of hemodynamic changes during sleep became an interesting research topic by itself [Publication III].

Materials and methods

A preliminary study was carried out to test the ability of the four-channel FD instrument to detect hemodynamic changes in the human brain during natural sleep. The series consisted of six recordings on two volunteers. One measurement was done at a single wavelength (808 nm) and the others at two wavelengths (760 and 808 nm) controlled by a DiCon prism switch (see Subsect. 3.4).

As in hyperventilation and breath-holding studies, a similar laser power and positioning of fiber holder with the same SDDs were used. In the first two measurements, the fibers touched the subject's skin and in the others, they were fixed approximately 1.2 mm above the skin. During $\sim$ 1.5 – 2.5-hour measurement, the subject lay in bed. The night before the measurement the subjects were asked to sleep some 2 to 3 hours less than normally to help them fall asleep for the measurement. The subjects were woken up at the end of recording. The ethics committee of the hospital approved the study plan.

As the reference method, polysomnography was used to classify the sleep stages of the subject (see Subsect. 3.7). The polysomnographic data were analysed by a professional neurophysiologist with the help of a semi-automatic classifier (Somnologica, Flaga hf. Medical Devices, Iceland) and following the Rechtschaffen and Kales rules [127]. The sleep stages were classified into six different categories: awake, sleep stages 1−4 (S1−S4), and the rapid eye movement (REM) sleep and into movement time (MT).

The low-frequency changes in single-wavelength I_{AC} data were enhanced by low-pass filtering and down-sampling the signals. For the dual-wavelength measurements, the wavelengths were switched at the frequency of $\sim$ 1 Hz. The I_{AC} data at both wavelengths were separately averaged over the pulses and temporally aligned. The [HbO_2] and [HbR] were calculated from the I_{AC} signals using the modified Beer Lambert law (Eq. 2.2). The DPF values were taken from the literature [73, 128] because the FD instrument was not calibrated for these measurements.

4.2.1 Results

The single-wavelength I_{AC} signals correlated well with the changes in the sleep stages [Publication III, Fig. 9]. The measurement was primarily sensitive to changes in the CBV at 808 nm. During the falling-asleep period, the amplitude signal increases indicating a decrease in the CBV. Correspondingly, during the waking-up period, the CBV increased decreasing the optical signal. Both the heart rate and the SaO_2 decreased during the sleep periods as well.

Figure 4.1 shows the data from a dual-wavelength sleep measurement. The [HbO_2]

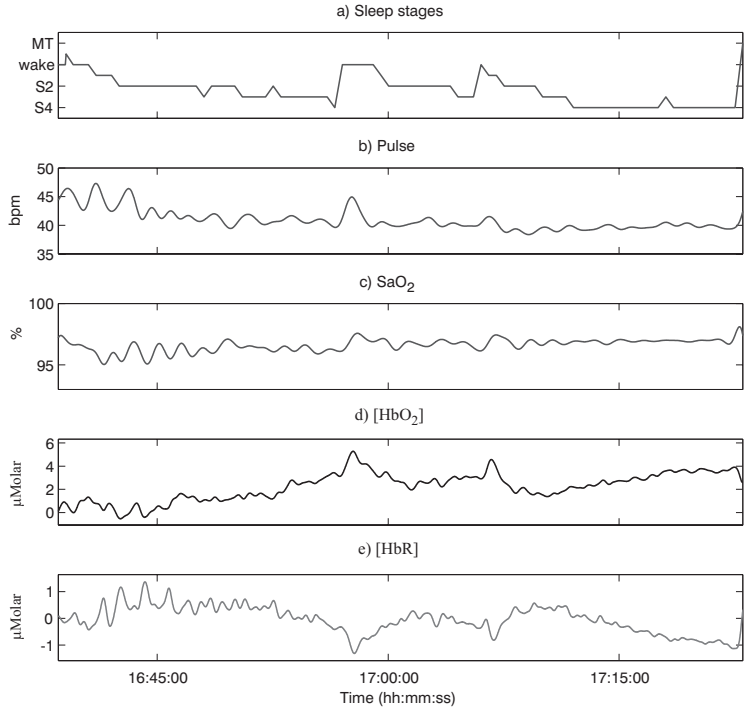

Figure 4.1: Data from dual-wavelength natural sleep measurement. The optical signals were measured using the SDD of 3 cm. The Δ[HbO_2] and Δ[HbR] signals were low-pass filtered using a time constant of 15 s to emphasize the slow changes in the signals. (Modified from Publication III)

increases and the [HbR] decreases during the two awakening periods around 16:58:00 and 17:08:00. The increase in the [HbO_2] is larger than the decrease in the [HbR] indicating an increase in CBF during awakening if $CMRO_2$ is assumed to stay constant. Changes in the HR are also detected during the awakening transitions.

4.3 Simultaneous NIRS and EEG measurements of the effects of baseline blood flow changes on visually evoked responses

EEG is a traditional technique to study the post-synaptic activity of neurons in the human brain [23]. In spite of its versatile applicability in human brain studies such as in the detection of epilepsy, EEG does not directly measure the cerebral hemodynamic and oxygenation changes. The neuronal and vascular processes in the brain are linked together by the so-called neurovascular coupling [33, 34].

Here, a method is introduced to study the system level neurovascular coupling by simultaneous NIRS and EEG measurements [Publication IV]. An integrated EEG-

NIRS helmet was implemented for these measurements. The main objective of this study was to investigate plausible relationships between the changes in baseline blood flow and the visually evoked hemodynamic and neuronal responses.

In addition to NIRS, only fMRI provides a comparable temporal resolution to study the time courses of hemodynamic responses non-invasively [40–42]. It is, however, technically more challenging to combine EEG with fMRI than with NIRS [129–131]. Some simultaneous NIRS and EEG measurements have already been reported [132–140, Publication IV]. This was the first study where the whole-head EEG and multi-channel NIRS were combined.

4.3.1 Materials and methods

For this study three volunteers were measured, and one of them (Subject 1) was measured twice. In the first session of Subject 1, a radial half-field pattern-reversed checkerboard stimulus was used. In all other measurements, 16-ms rectangular full-field checkerboard (24x32 cm) flashes were presented on a normal computer monitor. The stimulus blocks were $\sim$ 5-s long with an inter-stimulus interval of $\sim$ 0.5 s so that each block contained ten flashes or pattern reverses. The stimulus blocks were separated by $\sim$ 25-s rest blocks. Each subject participated in four visual activation measurements, two during normo- and hypocapnia and two during normo- and hypercapnia. The measurement sets were counterbalanced so that two measurements started with 4-min normocapnia and the other two with 4-min hypo- or hypercapnia periods in a random order. Hyperventilation was used to induce hypocapnia. Hypercapnia was produced by breathing CO_2-enriched air (see Subsect. 3.7). The study plan was approved by the ethics committee of the hospital.

The current configuration of our FD instrument including the new source system (see Sect. 3.4) was used in this study. Two wavelengths (760 and 830 nm) with $\sim$ 12 and 16 mW of output powers were applied. EEG signals were recorded using a 60 channel system compatible with TMS [141]. Multiple EEG channels enable us to localize the strongest visually evoked activity.

The optode holders were integrated into the EEG cap to make simultaneous measurements of optical and EEG responses possible (Fig. 4.2). One source fiber and eight detection bundles were placed on both left and right hemispheres above the visual cortex at three different SDDs ($\sim$ 35, 42, and 55 mm).

After preprocessing, the sampling frequency was $\sim$ 6.2 Hz for the optical signals. The signals from the closest source only were further analysed resulting in eight active detectors from both hemispheres. The data at different wavelengths were

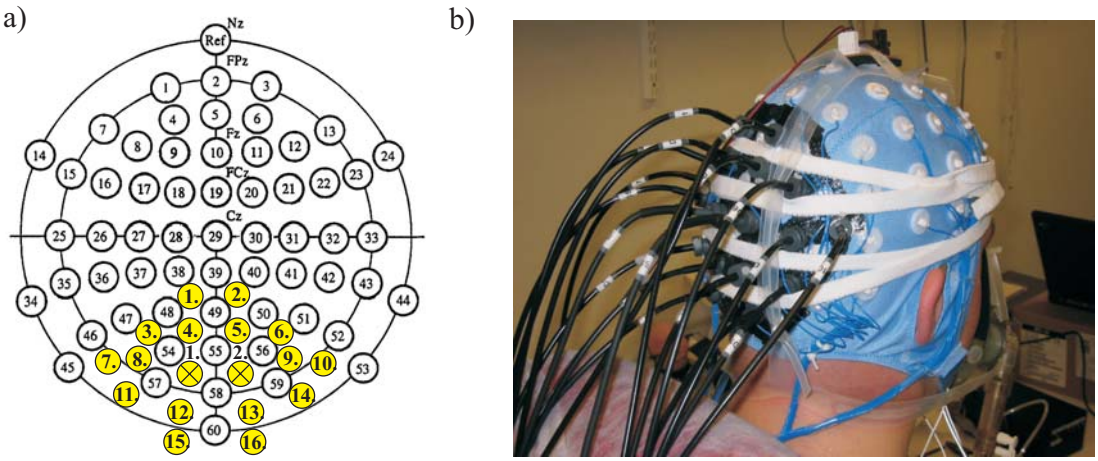

Figure 4.2: a) The positions of the 60 EEG electrodes, the 2 source optodes (yellow crosses), and the 16 detection optodes (numbered yellow circles). The locations of some electrodes from the International 10-20 electrode placement system are also shown. b) Photograph of the measurement setup. A movement sensor (see Subsect. 3.7) was also taped on the top of subject's head. (From Publication IV)

temporally aligned and the [HbO_2] and [HbR] signals were calculated using again the modified Beer-Lambert law (Eq. 2.2). Values from literature were used for the DPFs [73, 128]. Baseline changes in [HbO_2] and [HbR] due to hypo- and hypercapnia were investigated by low-pass filtering the signals ($f_{-3\,dB} = 0.0166\,Hz$). Before further averaging, the baseline changes were subtracted from the signals and the signals were again low-pass filtered ($f_{-3\,dB} = 0.5\,Hz$) to suppress the pulse component and other high-frequency interferences. The [HbO_2] and [HbR] responses were averaged using a window with a $\sim$ 5-s pre-stimulus interval and a total length of $\sim$ 35 s. The signals during normocapnia and hypo- or hypercapnia were processed separately resulting in eight responses altogether for each average from each data set.

The EEG epochs with clear artifacts were rejected. The averaging window started 70 ms before each stimulus and had a total length of 470 ms. The averages were low-pass filtered ($f_{-3\,dB} = 40\,Hz$). The stimulus blocks were divided into normocapnia and hypo- or hypercapnia intervals so that 80 epochs at maximum were averaged during each condition.

4.3.2 Results

The analyses of baseline changes during hyperventilation reveal similar decreases in [HbO_2] in all channels indicating a global decrease in CBF due to hypocapnia. During the recovery period, [HbO_2] increases close to its initial level. The changes

in [HbO_2] are small during the normal breathing period. When CO_2 enriched air is breathed, CBF increases and the changes in [HbO_2] are opposite to those during hypocapnic periods.

Hemodynamic responses evoked by the visual stimuli could be detected in all the 16 measurements. Channels 8 and 9 always provided the strongest responses [Publication IV, Fig. 5]. The [HbO_2] typically increases and [HbR] decreases during a response showing similar temporal behaviours to those reported in previous studies [37, 41]. The response peaks within $6 - 12$ s after the stimulus onset and is suppressed within 15 s. The upper four channels ($3 - 6$) typically showed clearer responses than the lower four channels ($11 - 14$). The SNR of the signals corresponding to SDDs of 5.5 cm was too low to reveal responses reliably.

The effects of hypo- and hypercapnia on the hemodynamic responses were easiest to detect on channels 8 and 9 where the SNR of the NIRS responses were highest. The interpretation was therefore focused on these channels (Figs. 4.3a-d and 4.4a-d). The changes in the peak amplitudes and latencies of the HbO_2 responses were studied. During hypocapnia, the peak amplitude of HbO_2 responses decreased in four and increased in one out of eight measurements. On the other hand the latency of HbO_2 responses became shorter in five and longer in one measurement during hypocapnia.

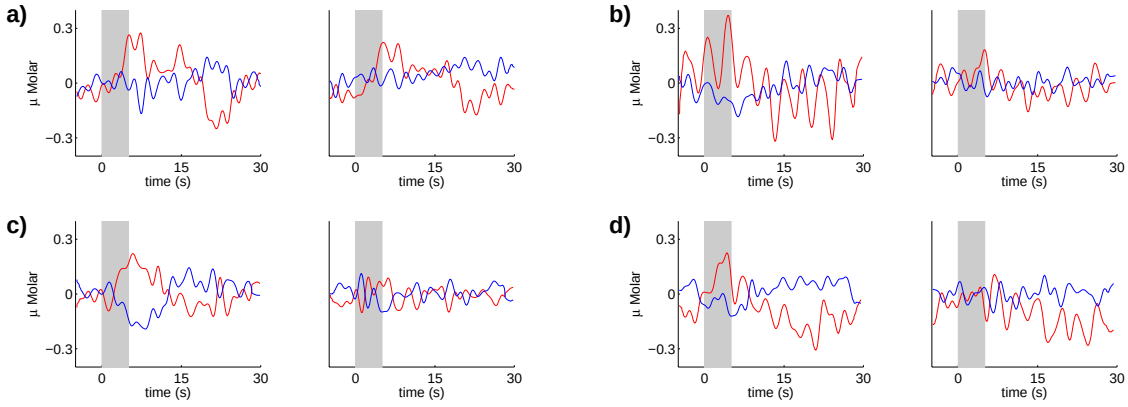

Figure 4.3: Hemodynamic signals averaged over eight responses (Subject 2) during normocapnia when (a) a hypocapnic period starts and (c) ends the measurement. The responses during hypocapnia when (b) a hypocapnic period starts and (d) ends the measurement. Red color represents [HbO_2] and blue [HbR] signal. In each image (a)-(d), the signals on the left are from channel 8 and right from channel 9. (From Publication IV)

The hemodynamic responses during normocapnia and hypercapnia are shown in Fig. 4.4a-d. During hypercapnia, the peak amplitudes of HbO_2 responses decreased

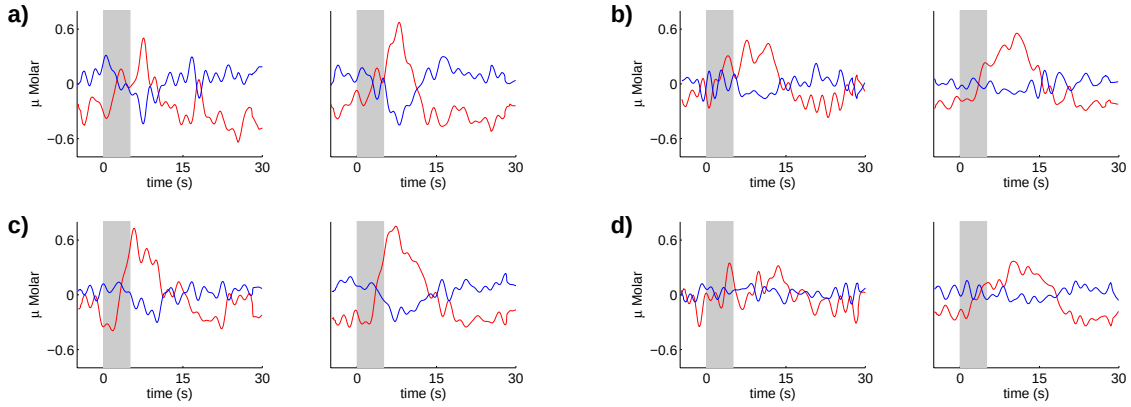

Figure 4.4: Hemodynamic signals averaged over eight responses (Subject 3) during normocapnia when (a) a hypercapnic period starts and (c) ends the measurement. The responses during hypercapnia when (b) a hypercapnic period starts and (d) ends the measurement. Red color represents [HbO_2] and blue [HbR] signals. In each image (a)-(d), the signals on the left are from channel 8 and right from channel 9. (From Publication IV)

in all except one measurement. The latency of HbO_2 responses became longer in all measurements during hypercapnia.

The visually evoked potentials (VEPs) were detected in all 16 measurements. The strongest responses originated in the channels 48−50 and 54−60 located above the visual cortex. The P100 component that arose $\sim$ 100 ms from the onset of stimulus was observed in all these VEPs [142]. The effects of hypo- and hypercapnia on the peak amplitude and latency of VEP-P100 component were also studied. These changes were typically easiest to detect in channels 58 and 60, which were selected for further analyses.

The peak amplitudes increased in four and decreased in two measurements during hypocapnia. The latency was shorter in six and longer in one hypocapnic measurement. During hypercapnia, the peak amplitudes decreased in four and increased in two measurements. The latency was shorter in five and longer in two hypercapnic measurements.

4.4 Effects of inhaled iloprost and additional nitric oxide on the cerebral and other circulatory parameters of preterm lamb

The pulmonary vascular resistance decreases rapidly during a normal postnatal transition from fetal to neonatal circulation. Disturbances in this transition may lead

to an elevated pulmonary arterial resistance resulting in a pulmonary hypertension (PH), low oxygen delivery to tissue and peripheral hypoxia. Nitric oxide (NO) and prostacyclin are one of the main endogenous pulmonary vasodilators [143]. Inhaled NO (iNO) is a widely accepted therapy for PH in newborns [144]. Because iNO is expensive and potentially toxic [145], it is important to study alternative pulmonary vasodilators, one of which is the prostacyclin analogue iloprost. Only some promising case reports exist on the circulation effects of inhaled iloprost in newborn infants [146–148].

For newborn lambs, hypoxia constricts the pulmonary vessels, inducing a condition similar to the persistent PH in newborns [149]. The main objective of this study was to test using a preterm lamb model [150] the effects of inhaled iloprost on the pulmonary and peripheral circulation including the cerebral hemodynamics monitored using NIRS. Also an iNO treatment was used to assess its additional effects on parameters studied. The benefits of NIRS to detect cerebral tissue oxygenation and hemodynamic changes were tested in this multimodal monitoring setup.

4.4.1 Materials and methods

19 preterm lambs delivered by caesarean section were studied. The lambs were randomized to iloprost or control groups. After the fetal head and neck were extracted, the head was covered by a rubber glove to transiently preclude breathing. Catheters were placed in the axillary artery and in the jugular vein for blood sampling. An ultrasonic flow probe was placed on the carotid artery. An endotracheal tube was inserted by tracheotomy and surfactant was given. After delivery, the lamb was weighed, moved to an incubator and an endotracheal tube was connected to the ventilator.

With the help of ultrasound, the venous catheter was inserted into the right ventricle to continuously monitor right ventricular pressure (RVP). Catheters were placed in the umbilical vein and artery for postductal blood sampling. From preductal and postductal blood samples, pH and blood gases were analysed. Three subcutaneous electrodes were used to continuously record ECG. A temperature probe and the NIRS probe of NIRO 300 (Subsect. 3.7) were attached to the scalp. A continuous tail pulse-oximeter was used to register SaO_2. Transthoracic echocardiography was performed to measure blood flow velocities in the aorta and proximal parts of the coronary arteries using a Doppler ultrasound probe. From these data the cardiac output was estimated.

After 60 min of stable ventilation, three 15-min iloprost doses in 15-min intervals were given using a nebuliser connected to the ventilator tubing. For the control

group, saline was administered. For the low dose group, the iloprost dose was doubled for each inhalation, whereas for the high dose group, the last dose was five-fold compared to that given for the low-dose group. An iNO dose of 40 ppm was given to lambs of the high dose iloprost group and to five control lambs after 90 min [Publication V, Fig. 1]. During iloprost treatment, all measurements were performed in seven time points; just before and 15 min after the onset of each inhalation and 30 min after the last inhalation. The 90-min values were also used as the baseline for iNO (before iNO) and the response values (during iNO) were recorded during the next 10 min.

Before attaching the NIRS probe above the temporal lobe the fetal head was shaved and cleaned. The longer SDD (5 cm) was preferred to maximize the contribution of cerebral signal. The [HbO_2], [HbR], and Cyto-Ox signals, and TOI were acquired at 0.2 Hz sampling rate.

During iloprost treatment NIRS data were sampled at every 15 min simultaneously with other parameters. NIRS signal artifacts were corrected using an algorithm. To quantify the signals a DPF previously used for fetal lambs was utilized [151]. Concentration changes in [totHb] were also analysed. The original TOI signal was normalized with its baseline value before the first iloprost or saline inhalation, or iNO to derive relative TOI values. The before iNO values were averaged in the window between 4 and 2 min before the onset of iNO and the during iNO values in the window between 8 and 10 min after the onset of iNO.

The preprocessing and statistical analyses were carried out in Matlab programming environment (The MathWorks, Inc.) and with SPSS software (SPSS, Inc.).

4.4.2 Results

Statistical analyses revealed significant differences between the groups between 0 and 60 min only in haemoglobin ($p=0.021$) and TOI ($p=0.050$). However, no significant differences between the groups in changes over time (0-60 min) were observed in any parameters. It was also found that the third iloprost inhalation did not affect significantly on physiological parameters.

The NIRS data obtained from the low and high iloprost groups were similar (Fig. 4.5). From 45 to 90 min a significant decrease ($p<0.025$) occurred in [HbO_2] and in relative TOI in control lambs, whereas no such change was observed in the iloprost treated lambs (Fig. 4.5). The [totHb] correlated significantly ($R^2 = 0.14$, $p<0.001$) with haemoglobin values, whereas [HbO_2] did not.

An evident increase in oxygenation occurred in both groups during iNO treatment

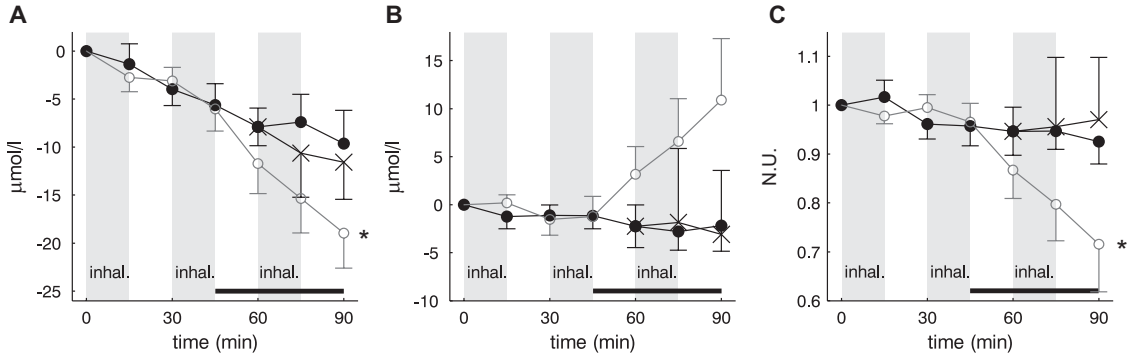

Figure 4.5: Effect of inhaled iloprost (grey areas) on cerebral tissue oxygenation. ○ saline (n=10), × low iloprost (n=3), and ● high iloprost (n=5) group. (A) A decrease in [HbO_2] and (C) in relative TOI (normalized unit, N.U.), and (B) an increase in [HbR] occurred only in control lambs indicating the degrade of cerebral oxygenation. The changes in [HbO_2] and relative TOI from 45 to 90 min (solid thick line) differ significantly (* $p<0.025$) between control and iloprost groups. (From Publication V)

which was shown as significant changes in several parameters. However, only RVP decreased significantly more ($p<0.01$) in iloprost than in saline pretreated lambs [Publication V, Fig. 3]. [HbO_2] increased and [HbR] decreased during iNO indicating a significant increase in cerebral oxygenation (Fig. 4.6).

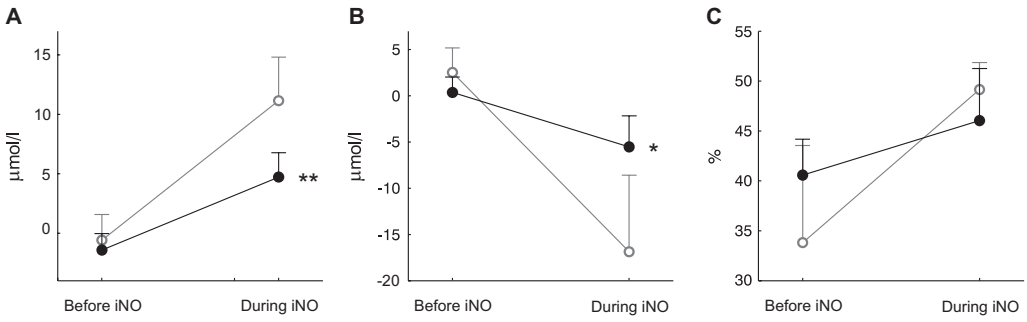

Figure 4.6: During iNO (A) the [HbO_2] increased in control and iloprost groups and (B) [HbR] decreased correspondingly (* $p<0.05$, ** $p<0.01$). (C) However, TOI did not increase significantly (○ saline+iNO, n=4 and ● iloprost+iNO, n=5). (From Publication V)

5 Pathlength measurement in detection of source coupling error in near-infrared spectroscopy on human forehead

Currently there is no widely used method in NIRS to directly measure the quality of coupling between source optode and tissue and thereby measurement reliability. This is probably one of the reasons why NIRS methods have not been widely accepted in clinical practice [10–12]. Previously, coupling errors have been compensated in imaging experiments by using special reconstruction methods [152, 153]. In this study, the linearity of absolute ϕ, quasiabsolute I_{AC}, and I_{DC} in human forehead measurements is analysed as a function of SDD. Previously, the linearity of these variables has mainly been demonstrated in phantom studies [58, 71, 84–86, 154–161].

The temporal information such as ϕ data in NIRS has been typically used in three different ways. The mean pathlength of photons in tissue can be determined from ϕ data and used to quantify the concentration changes in tissue with the help of, e.g., the modified Beer-Lambert law (Eq. 2.2). In frequency-resolved spectroscopy, the ϕ data have been used to solve the DE analytically and to derive the estimates of the absolute values of [HbO_2] and [HbR] [4, 85, 86]. In optical tomography the ϕ and I_{AC} or I_{DC} measurements are required for the reconstruction of the spatial distributions of μ_a and μ_s' independently [61, 93].

Based on ϕ data a novel approach to detect an incomplete source-to-tissue coupling in a forehead measurement will be introduced. The effects of a bad coupling on the contrast and depth sensitivity of [HbO_2] and [HbR] responses during hypercapnia and hyperventilation are also investigated.

5.1 Instrumentation and data calibration

In this study, our FD instrument included the laser diodes at 760 and 830 nm, the 1×2 prism switch for wavelength selection and the 1×16 moving fiber switch for selecting the source position (Subsect. 3.4 and [Publication II]). Two source fibers and ten detector bundles were attached on two parallel rows between $\sim 1-5$ cm on the right side of the forehead using a same individually shaped fiber holder for each subject. In this special fiber holder, every other source and detector terminal had a gap ($\sim$ 1.6 mm) between the optode and tissue. Half of the optodes were thereby pushed against the fiber holder material while the others made a contact with skin. This arrangement made it possible to investigate the influence of non-contact optode

on the FD measurement parameters.

To produce absolute ϕ and quasiabsolute I_{AC} data the FD instrument was calibrated using a three-step procedure [Publication II]. In the first step, the effects of HV changes in PMTs on the ϕ and I_{AC} signals were corrected at both wavelengths using an independent phantom measurement. In the second step, the interchannel variations of each source and detector channel were balanced against source 1 and detector 1 [67]. Finally, the ϕ and I_{AC} values between source 1 and detector 1 were measured just before or after each measurement. For the I_{DC} data, only HV changes were compensated with the estimated gains of the PMTs. The data acquisition cards of the FD instrument corresponding to detection channels 9 and 10 were not precisely synchronized, which prevented exact ϕ calibration of these channels.

5.2 Study design

All measurements started with a 2-min rest period, during which the values for the regression analyses were measured. This was followed by three 2-min periods when the subject either breathed CO_2 enriched air or hyperventilated resulting in either hyper- or hypocapnia (Subsect. 3.7). After each breathing period, a 4-min rest period followed so that the total measurement time was 20 min. Hypercapnia increases the CBF elevating the [HbO_2] and reducing the [HbR] provided that the oxygen consumption stays constant. For hypocapnia the opposite happens.

Measurements were carried out on 10 volunteers, one of which was measured twice. The subjects had two hypercapnia and two hyperventilation measurements in a random order. Finally, 43 measurements were used for this study. When appropriate, the results were analysed using paired (p_1) or unpaired (p_2) parametric or non-parametric statistical tests. The ethics committee of Helsinki University Central Hospital approved the study protocol and all the subjects signed a written consent before the measurements.

5.3 Data preprocessing and linear regression of calibrated variables

The raw $ln(I_{AC})$, ϕ and $ln(I_{DC})$ data were calibrated, after which a phase wrap was removed. Data at different wavelengths and those corresponding different sources were averaged separately resulting in ~ 0.47 Hz sampling rate for final signals. The influence of the small gap below some of the optodes on the ϕ signals was corrected.

To study the linearity of FD variables, the regression analyses were carried out using

data averaged over the first 2-min rest period. The I_{AC} and I_{DC} values were simply linearized by taking the natural logarithm of them. In tissue or tissue-like materials the FD measurement variables show nonlinear SDD dependence at SDDs < 20 mm so that detection channels 1 and 6 were excluded from the analyses [128, 162, 163]. In addition, calibration could not be carried out for detection channels 9 and 10. As a result, data from detection channels $2-5$ and $7-8$ corresponding to SDDs between 2 and ~ 5.1 cm were analyzed using linear regressions with least squares.

The differences in the calibrated ϕ, $ln(I_{AC})$ and $ln(I_{DC})$ values between different wavelengths and different sources were tested. Because generally the values of all parameters at different SDDs differ significantly, the regression analyses were carried out separately for data corresponding to different sources and different wavelengths.

For both sources and both wavelengths the coefficients of determination (R^2) for $ln(I_{AC})$ were on average ~ 0.99 and for $ln(I_{DC})$ ~ 0.97 - 0.98. For the ϕ data the R^2 values were clearly smaller especially for the non-contact source 2 they were only ~ 0.76.

5.4 A criterion to detect a low-quality measurement value

Because the calibrated variables tended to behave linearly, an assumption was made that the values in all technically successful measurements should show a high linearity as a function of SDD. The R^2 parameter was chosen to represent the quality of linearity. A R^2 value of 0.95 corresponding to $p = 0.001$ of the statistical F-test in a six sample regression analysis was selected to be the threshold.

An empirical criterion was derived to classify the calibrated data as good- and low-quality values. First, all the measurements with a regression above the threshold were selected. The mean values and STDs of slopes ($b_{mean,s,l}$ and $b_{STD,s,l}$) and y-intercepts ($i_{mean,s,l}$ and $i_{STD,s,l}$) of these measurements were determined separately for each variable in each source (s) and at each wavelength (l). If an individual value ($y_{s,l}$) at a certain measurement distance SDD did not lie between the upper and lower limits,

$$\begin{aligned} y_{s,l}(SDD) &\geq (b_{mean,s,l} - b_{STD,s,l}) \cdot SDD + (i_{mean,s,l} - i_{STD,s,l}) \text{ and} \\ y_{s,l}(SDD) &\leq (b_{mean,s,l} + b_{STD,s,l}) \cdot SDD + (i_{mean,s,l} + i_{STD,s,l}), \end{aligned} \tag{5.1}$$

and it belonged to a set with regression below the threshold, it was classified as a low-quality value. Otherwise it was classified as a good-quality value.

The regression of classified variables

The classification criterion was applied to $ln(I_{AC})$, $ln(I_{DC})$, and ϕ data. All the $ln(I_{AC})$ values were assigned to the good-quality class and only 2.6% of $ln(I_{DC})$ values were assigned to the low-quality class almost equally from both sources. The criterion based on $ln(I_{AC})$ or $ln(I_{DC})$ data is therefore not able to detect possible changes in a source-to-tissue coupling. However, 21.8% of the ϕ values were classified as low-quality and 83% of them were from source 2. When the regression analyses were carried out for the ϕ values corresponding to the good-quality measurements, all the data sets had $R^2 > 0.95$ and the mean R^2 values of both sources at both wavelengths were ~ 0.99.

A light leakage caused by a coupling error

If the I_{AC} and I_{DC} data are divided into low- and good-quality classes according to the classification of ϕ data, significantly higher ($p_2 < 0.05$) $ln(I_{AC})$ and $ln(I_{DC})$ levels were obtained in 9 out of 12 SD pairs for source 2. This finding indicates that the low regression ϕ values are due to a light leak through the surface tissue. The high sensitivity of regression of ϕ values to a leak from source to detectors can also be simulated. If the same $ln(I_{AC})$ bias is added to all otherwise linear values at the different SDDs, the regression of ϕ becomes worse but that of $ln(I_{AC})$ remains practically the same.

5.5 The effects on the quality of physiological responses

The results of regression analyses were used to classify the [HbO_2] and [HbR] responses to good- and low-quality classes. The concentration changes were estimated from the $ln(I_{AC})$ data using the modified Beer-Lambert law (Eq. 2.2). The DPFs were derived assuming that the measured ϕ is directly proportional to the mean pathlength of photons in tissue [58].

The detector channels 5 and 10 with the longest SDD have the longest partial pathlength through the brain tissue [164]. Then the cerebral responses should be most pronounced on those channels [100, 165, 166]. Because the calibrated ϕ data were not available for detection channel 10, only detection channel 5 was chosen for further analyses. All the [HbO_2] and [HbR] signals showing clear movement artifacts were rejected.

The light leak is assumed to take place only in the tissue surface, which does not

contribute to the physiological changes induced by breathing exercises. The non-leaking part of photons should propagate approximately through the same path as the photons in measurements without a leak. Then in the estimation of [HbO_2] and [HbR] signals in measurements with bad coupling, the actually measured short DPFs can be replaced with the mean DPFs of measurements without a leak.

Classification of signals

If one or both wavelengths produced a low-quality ϕ value, that particular SD pair was classified as low-quality. Differences were tested between measurements which included only one low-quality SD pair. This made it possible to compare the low- and good-quality SD pairs of same subject to each other removing the effect of intersubject variability on the results.

After classification, in each of the 16 partly corrupted measurements, source 1 always produced a good-quality and source 2 always a low-quality ϕ value. Because different sources sample somewhat different spatial regions, all measurements with a good-quality ϕ value from both sources were selected for reference purposes.

Parameters calculated from the physiological responses

If a measurement contains a low-quality calibrated ϕ value, the quality of physiological responses is likely to be affected as well. To test this assumption, four parameters, contrast, noise level, CNR and area-under-the-curve (AUC) were calculated from the [HbO_2] and [HbR] responses of channel 5 separately for both sources.

From each measurement three contrast, CNR and AUC values were calculated, because each measurement included three responses. By reversing the sign of the contrast, CNR and AUC values the hyperventilation parameters were combined with the hypercapnia parameters. Only the responses having CNR > 1.5 were included in the analyses. For AUC values, approximately the same number of responses was included to the analyses as in the case of CNR and contrast. All four noise segments from each measurement were utilized.

Comparison of parameters between groups

The mean values and STDs of each parameter were calculated using the measurements of good- and low-quality groups and over the source 1 and source 2 groups separately (see Table 5.1).

Table 5.1: Signal features divided into the different groups (good and low / source 1 and 2) using the ϕ classification. The mean values and STDs over all parameters of each group are given. (From Publication VI)

	Contrast	AUC	Noise	CNR
$[HbO_2]_{good}$	2.25 ± 1.89 $^{\|\|,\dagger}$	0.77 ± 0.53 $^{\|\|,\ddagger}$	0.65 ± 0.26 $^{\|\|,\ddagger}$	3.45 ± 2.62 **
$[HbO_2]_{low}$	1.57 ± 1.55	0.51 ± 0.45	0.55 ± 0.30	2.82 ± 2.27
$[HbR]_{good}$	1.11 ± 0.46 $^{\|\|,\$}$	0.42 ± 0.18 $^{**,\$}$	0.35 ± 0.13 $^{\|\|,\dagger}$	3.31 ± 1.60 $^{\|\|,\ddagger}$
$[HbR]_{low}$	0.55 ± 0.49	0.26 ± 0.13	0.30 ± 0.13	1.78 ± 1.73
$[HbO_2]_{s1}$	3.00 ± 1.41 *	0.88 ± 0.45 **	0.94 ± 0.25	3.41 ± 1.84 **
$[HbO_2]_{s2}$	2.67 ± 1.43	0.77 ± 0.50	0.95 ± 0.23	3.03 ± 1.84
$[HbR]_{s1}$	1.27 ± 0.48 $^{\|\|,\dagger}$	0.45 ± 0.14 $^{\|\|,\$}$	0.49 ± 0.14	2.98 ± 1.35 **
$[HbR]_{s2}$	0.97 ± 0.60	0.31 ± 0.21	0.48 ± 0.14	2.40 ± 1.53

$^{*}p1 < 0.05$, $^{**}p1 < 0.01$, $^{\|\|}p1 < 0.001$

$^{\dagger}p2 < 0.05$, $^{\ddagger}p2 < 0.01$, $^{\$}p2 < 0.001$

The contrasts and AUCs of both $[HbO_2]$ and [HbR] signals were significantly higher in the good-quality than in the low-quality group. The values for these parameters were also higher in the source 1 than source 2 group. The differences between the source 1 and source 2 groups are smaller and not as significant as between the low- and good-quality groups. This means that part of the contrast and AUC differences between groups are due to the fact that sources 1 and 2 probed spatially different volumes. However, if source 2 has a bad coupling, the contrast and AUC differences increase.

Furthermore, the noise level of $[HbO_2]$ and [HbR] signals in the low-quality group is smaller than in the good-quality group, whereas the noise levels are practically the same in the source 1 and 2 groups. Because the leaking light has a low physiological noise level, a light leak decreases the noise level. However, the additive leaking noise component severely decreases the contrast.

The CNRs are clearly higher in the good-quality than in the low-quality group. On the other hand, the CNRs are only slightly higher in the source 1 group compared to the source 2 group. Thus if a source has bad coupling, also the CNR of physiological responses decreases.

5.6 The effects on the depth sensitivity

A low-quality ϕ value is an indication that the light probes the surface tissue more than it normally should. Therefore, such responses measured at SDDs $\geq$ 5 cm should be similar to those measured at SDDs $<$ 2 cm. This assumption was tested by calculating the Pearson's correlation coefficients (CC) and standardized mean squared errors (sMSE) of the [HbO_2] or [HbR] signals from detector channels 5 and 1 separately for measurements containing low- and good-quality ϕ values. The CCs were significantly higher and sMSEs lower in the low-quality when compared to the good-quality measurements for both [HbO_2] and [HbR] signals. Therefore, the signal waveforms obtained at different SDDs resemble each other more in low-quality measurements.

The good- and low-quality responses of channels 5 and 1 were also qualitatively compared (Fig. 5.1 and Fig. 5.2). Before averaging, the baseline values of responses were

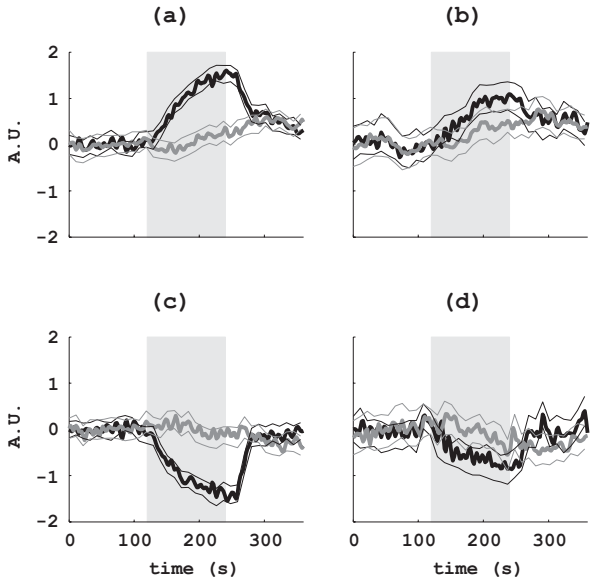

Figure 5.1: Standardized [HbO_2] signals from a) good- and b) low-quality hypercapnia measurements. Standardized [HbR] signal from c) good- and d) low-quality hypercapnia measurements. The signals of detector channel 1 are presented with a grey color and the signals of detector channel 5 with a black color. Thin lines represent 95% confidential intervals. The period of breathing exercise is indicated with a light grey color (A.U. = arbitrary units). (From Publication VI)

shifted to zero and the responses were divided by their STDs to standardize their waveform variations. The [HbO_2] and [HbR] responses were averaged separately from all good- and low-quality hypercapnia and hyperventilation measurements.

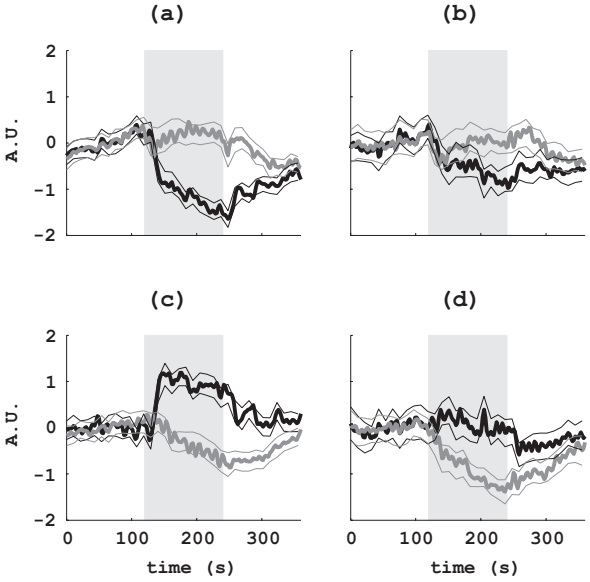

Figure 5.2: Standardized [HbO_2] signals from a) good- and b) low-quality hyperventilation measurements. Standardized [HbR] signals from c) good- and d) low-quality hyperventilation measurements. The signals of detector channel 1 are presented with a grey color and the signals of detector channel 5 with a black color. Thin lines represent 95% confidential intervals. The period of breathing exercise is indicated with a light grey color (A.U. = arbitrary units). (From Publication VI)

During hypercapnia, good-quality measurements at SDD $\sim$ 5 cm showed evident increase in [HbO_2] signals. At SDD $\sim$ 1 cm the effect is not so clear. In addition, a clear decrease in the [HbR] signals in good-quality measurements is seen at SDD $\sim$ 5 cm whereas at SDD $\sim$ 1 cm no changes are observed. In contrast, in the low-quality ϕ measurements the responses at both SDDs are rather difficult to distinguish from the background noise without the prior information on breathing periods. During hyperventilation, similar but even more evident differences between the responses of good- and low-quality ϕ measurements are obtained.

6 Discussion

6.1 Instrumentation

Our FD instrument is primarily developed for tomographic imaging. However, it also provides an excellent SNR useful in quantitative NIRS at long (> 3 cm) SDDs. The system is able to measure absolute values of $ln(I_{AC})$ and ϕ with high accuracy and simultaneously acquire signals from multiple SD pairs at high sampling rates which are necessary in functional studies of brain hemodynamics. Other tomographic instruments have not provided such combination with as good features as our instrument [15–17, 60, 68]. Our system has versatile applicability and higher repeatability of I_{AC} and ϕ measurements and a faster measurement time compared to other published FD tomographic systems [60, 68]. Our FD instrument can also be applied to absolute imaging studies [Publication II] whereas other tomography systems have been mostly used for difference imaging [60, 66, 167, 168].

Preamplifiers

16 IF preamplifiers were implemented for the detection channels. Their noise levels fulfilled the requirements. Any interchannel crosstalk was not observed. High interchannel isolation is crucial in tomographic applications where the magnitude of signals in the adjacent channels may differ by several orders of magnitude. The isolation of preamplifiers to adjacent channels (> 98.1 dB) is sufficient in terms of tomographic measurements as well.

However, the performance of preamplifiers can still be further improved. A second-generation IF amplifier was recently implemented including a digitally adjustable gain, a truly differential input stage using INA and an active filter of high quality factor [169]. These improvements further decreased the output noise level of preamplifier to approximately one third of that of the current amplifiers.

A source system with four wavelengths

The FD instrument was further developed by implementing a four-wavelength source system. The new MEMS switches make possible the multi-source and multi-wavelength measurement of physiological processes at several Hz sampling frequency. The wavelength switch did not induce any extra noise to measured signals. The maximum interchannel leak in the switch is approximately -65 dB, and on average it is below -80 dB. The present interchannel isolation level should be sufficient for source multiplexing in tomographic applications if the optode positions are selected

in such a way that the crosstalk would be minimized. Also a custom-made MEMS switch possessing the required isolation across all channels might be possible to implement.

The performance of the temperature stabilizers was tested at room temperature. Temperature variations in the stabilized laser housings were $\sim$ 0.1-0.3 mK, which ensures sufficient stability for the FD instrument. In addition, the new circuit has several electrical and mechanical improvements over previous one.

Optode terminals for multimodal measurements

The detector and source fibers with prism terminals have proven their usefulness in several applications. They enable the attachment of optodes to the forehead of the subject in the supine position. They seem to be also less sensitive to motion artifacts than our cylindrical terminals. The prism terminals were successfully used in the sleep study [170]. The terminals have also made it possible to implement a bilateral TMS-EEG $-$ NIRS measurement series [171].

6.2 Brain measurements

Hyperventilation and breath-holding studies

The I_{AC} signals were shown to have larger contrasts and lower noise than the ϕ signals. The CNR of the I_{AC} signals also increased with increasing SDD. The noise in these signals was mainly due to the relatively large measurement bandwidth which could be straightforwardly reduced by low-pass filtering. Physiological changes and changes in measurement conditions limit the comparability of results at different wavelengths. In future measurements at different wavelengths should be carried out simultaneously.

Because a breath-holding exercise is a practical way to produce a large contrast in NIRS signals, it has also been used to study, e.g., changes in cerebral hemodynamics caused by ageing and by migraine [172, 173]. The hemodynamic changes caused by breath holding and the reproducibility of these responses have also been studied recently using fMRI [174].

The pulsating oscillations of optical signals have been utilized in a cerebral reflection pulse-oximeter and for the estimation of the pulsatile component of CBF and CBV [101, 175]. The SaO_2 parameter is also needed for modeling the $CMRO_2$ based on NIRS data [176]. The frequency range of VLFO reported here is slightly lower than those reported by other groups [117, 119, 177, 178]. These VLFOs may help in

the separation of NIRS signals originating from arterial and venous compartments of blood circulation. Suppression of such VLFOs improves the CNR in optical activation studies [119]. The temporal information of the oscillations might also be helpful in tomographic modeling [179, 180].

Similar hemodynamic oscillations, often known as the Mayer waves, can also be detected with other techniques such as blood-pressure, heart-rate variability and ultrasound measurements [118, 181, 182]. Multimodal setups may be helpful in interpreting the oscillations of optical signals and revealing their physiological origin [183].

Natural sleep studies

NIRS provides a novel method to study sleep and its disorders such as sleep apnea [96–98, 170, 184, 185]. In this study, changes in [HbO_2] and [HbR] were detected during the falling asleep and awakening periods in both single- and dual-wavelength measurements. These changes occurred, however, synchronously with changes in HR and SaO_2. These reference parameters have not been utilized before in data interpretation of other NIRS studies of natural sleep [96–98]. In future it would be therefore important to study whether NIRS can measure local cerebral changes which are not coupled with changes in systemic circulation. The multimodal setup of this study, including an ECG and a pulse oximeter, provides an excellent starting point for such studies. Recently a similar setup at the BioMag laboratory has been employed in two over-night natural sleep series [170, 186].

We detected decreases in [HbO_2] and increases in [HbR] during transitions from awake state to sleep and opposite changes during awakenings. Somewhat contradictory NIRS results have been reported by other groups [96–98]. In [98] no significant [HbO_2] or [HbR] changes were detected in the frontal lobe during the transitions from S1 to S2 or from S2 to S1. In [97] parallel changes in [HbO_2] and [HbR] were recorded during these transitions. Our results resemble most closely the results reported in [96].

Coupling of visual NIRS and EEG responses with a baseline blood flow

The neurovascular coupling has been an intensive topic of research during the last decade [21, 34]. A new technique was presented for the simultaneous measurement of VEPs and hemodynamic responses using whole-head EEG and multi-channel NIRS during normo-, hypo-, and hypercapnia. In other integrated NIRS and EEG measurements, just a single or a few EEG electrodes and lower number of optodes have been used [132–139,187]. Before this study, the visual stimulation was used only

in one concomitant study [133] whereas afterwards several studies have employed a visual stimulus [136–139]. In a couple of studies, NIRS responses have also been recorded simultaneously with MEG [188, 189]. With a whole head EEG or MEG and multi-channel NIRS, the localization of responses with the highest contrast is possible. A similar setup has been recently used to study the linearity between the hemodynamic responses and VEPs to different stimulus lengths from 3 to 12 s [140]. The implemented NIRS-EEG helmet is also TMS compatible so that combined TMS-EEG − NIRS measurements are possible [171].

In our study, the effects of hypo- and hypercapnia on the hemodynamic responses were investigated with NIRS for the first time. Previous hypo- and hypercapnia NIRS studies have measured only the baseline changes in [HbO_2] and [HbR] [100,165, 190, 191]. Hypo- and hypercapnia were shown to generate consistent latency shifts in visually evoked hemodynamic responses. Similar delays in BOLD responses have been observed using fMRI [192]. The measurement setup of this study provides an excellent starting point for further investigations of the unknown physiological origin of these delays. During hypo- and hypercapnia the observed amplitude changes of hemodynamic responses were not consistent and they may even be caused by the combined effect of latency changes and data averaging. The changes in the peak amplitude and in the contrast of hemodynamic responses caused by hypo- and hypercapnia have also been previously studied using fMRI [193].

The latency of VEP-P100 consistently decreased during hypocapnia. In previous studies, a reduction [194, 195] as well as an increase of latency of VEP-P100 [196] caused by hyperventilation have been reported. Furthermore, in some of our hyperventilation measurements, the increase of VEP-P100 amplitude was detected. This effect cannot be explained by averaging of VEPs with different latencies. Also during hypercapnia decreases in latencies and increases in VEP-P100 amplitudes were observed but not consistently. The reason for these inconsistencies may be the relatively small number of measurements.

Circulatory effects of inhaled iloprost and iNO on preterm lambs

The functional cerebral studies on newborn infants are one of the most attractive brain measurement applications of NIRS [76, 78, 79, 88, 197]. Their popularity is based especially on the safety of NIRS techniques.

In this work the beneficial effects of inhaled iloprost and iNO on the pulmonary and systemic circulation of newborn lamb were studied using a multimodal monitoring setup including a NIRS instrument. No significant differences were observed between the medicated study group and the control group in pulmonary or systemic

parameters during the entire iloprost treatment. However, the cerebral oxygenation decreased gradually after the 45 min of monitoring of the control lambs whereas for the iloprost treated lambs it remains practically constant. Furthermore, during an additional iNO treatment, an evident improvement in oxygenation was detected with several methods including NIRS. In RVP this change was significantly larger in the iloprost compared to the saline pretreated group. NIRS was shown to be a promising non-invasive method for direct monitoring of cerebral oxygenation and hemodynamic changes.

In these measurements carotid flow (CF) was used to detect differences in a global CBF between the groups. An increased CF and partial pressure of CO_2 in the iloprost lambs seem to improve the cerebral oxygenation [Publication V]. In contrast, in the low iloprost group SaO_2 showed low values especially at 90 min while the TOI parameter revealed relatively stable cerebral oxygenation. These differences may be explained, e.g., by the increase of oxygen extraction in the brain of low iloprost lambs compared to the controls. Even though the cerebral oxygenation detected using NIRS is significantly improved during iNO, CF did not produce consistent changes in either group. The [totHb] correlated significantly with the haemoglobin concentration measurement from blood samples during iloprost treatment indicating that the global reduction of concentration of haemoglobin produces a decrease in the cerebral concentration of haemoglobin which is detectable using NIRS. The new parameter, the relative TOI, was proved to be useful when changes between the groups were compared with respect to some arbitrary baseline values.

In this study, the movements and loosening of the measurement probe produced some artifacts in signals even though the lamb was anaesthetized, kept as still as possible and the probe was firmly attached. These artifacts are typical in NIRS applications [112, 113]. Here signal post-processing methods were used to remove such artifacts and generally improve the signal quality. The method to detect the quality of source-to-tissue coupling [Publication VI] may help to reduce problems arising from these kinds of artifacts in future.

6.3 Detection of source coupling errors

Linearity of FD measurement parameters

In NIRS measurements $ln(I_{AC})$, $ln(I_{DC})$ and ϕ should show a strong linearity as a function of SDD at $\sim 2-5.1$ cm. The fraction of variance unexplained (FVU = 1-R^2) with the linear regression model should be $\sim 1.0\%$ for all these variables [Publication VI]. Such linearity has been shown both theoretically and experimentally in several studies based on phantom data [58, 84–86, 154–161]. In some studies $ln(SDD \cdot I_{AC})$

and $ln(SDD \cdot I_{DC})$ rather than $ln(I_{AC})$ and $ln(I_{DC})$ have been shown to have linear SDD dependence [84–86, 157, 160, 161]. Our data shows that the linearity degrades from $R^2 = 0.992 \pm 0.007$ to $R^2 = 0.990 \pm 0.008$ when a regression is calculated using $ln(SDD \cdot I_{AC})$ instead of $ln(I_{AC})$ data [Publication VI].

In human studies, relatively constant DPF values have been measured on the forehead at SDDs > 2.5 cm [128]. The linear behaviour of mean pathlength at SDDs > 2 cm [92], as well as $ln(I_{AC})$ and ϕ data [198] on the human forehead has also been shown qualitatively.

Sensitivity of measurement parameters to coupling errors

If a source terminal has a loose contact to tissue, the regression of ϕ values can clearly decrease. However, regressions of the $ln(I_{AC})$ and $ln(I_{DC})$ data are not as sensitive to the source coupling errors as the regression of ϕ values. Previously the slope of ϕ data has been shown to change more than the slope of $ln(I_{AC})$ data if a clear layer representing cerebrospinal fluid (CSF) is immersed close to the surface of otherwise homogeneous phantom [158]. Monte-Carlo simulations show that if the scattering coefficient of CSF is changed, large differences in pathlength values can be observed in a multilayer head model [92]. In a recent study, the unrealistically short DPFs (< 2) measured on the human forehead at SDD = 5.7 cm were reported referring to errors between optodes and tissue [198].

In this study all the optode terminals were carefully attached on the forehead and a bad source coupling was discovered only during data postprocessing. However, 53% of ϕ measurements of source 2 and 14% of source 1 provided a low-regression at both wavelengths at SDDs $\geq$ 5 cm. Furthermore, the ϕ values were relatively constant throughout a single study session.

A classification criterion

A bad coupling between an optode and tissue can be detected using the criterion introduced. Nonlinearity of FD variables have also been used to reject data in the infant head measurements [88]. However, they used the same threshold ($R^2 < 0.97$) for all the optical raw data and did not report any differences between the linearity of ϕ and $ln(I_{AC})$ or $ln(I_{DC})$ data.

Because the variations of slope values in the regression analyses of ϕ data were rather small, the ϕ limits could be converted to nearly constant DPF limits. Thus a simpler criterion could be derived to detect the coupling using the DPF values only. This could open up the possibility to monitor the source coupling also with simpler instrumentation than used in our study [199].

6.4 Closing remarks

The development of an accurate FD imaging device requires careful design and implementation. Special emphasis should be placed on the development and testing of instruments before transitions to large clinical trials. The applied studies in the future will assess whether our FD instrument will facilitate the development of new clinically useful NIRS applications.

The brain studies of this work showed the potential of the developed instrumentation and the applied methods to reveal physiologically interesting information about the human brain not detectable using other modalities. The hemodynamic oscillations observed open up new ways to investigate novel physiological processes in tissue and to develop parameters especially for long-term monitoring. When the hemodynamic and oxygenation changes can be detected reproducibly, reliably and in a user-friendly way from the human brain using NIRS techniques, they will provide considerable clinical benefits especially in infant studies and in the monitoring studies in operation rooms and critical care units.

In this work, NIRS was used mostly as an independent method within the multimodal measurement setups. In the future, the signals from different modalities will probably be integrated using digital signal processing methods and new parameters will be developed based on the data of several modalities. This development may reveal new clinically useful information about complex physiological processes such as from the neurovascular coupling. The reliability and repeatability of individual measurement techniques can also be improved by utilizing multimodal approaches.

The developed method to detect problems in source-to-tissue coupling may prove to be very useful in future studies. It may prevent the acquisition of unreliable signals and improve the repeatability and usability of forehead NIRS measurements in general.

References

[1] F. F. Jöbsis. Noninvasive, infrared monitoring of cerebral and myocardial oxygen sufficiency and circulatory parameters. *Science* **198**:1264-1267, 1977.

[2] M. Cope. *The development of a near infrared spectroscopy system and its application for non invasive monitoring of cerebral blood and tissue oxygenation in the newborn infant.* PhD thesis, University of London, 1991.

[3] Y. Hoshi and M. Tamura. Detection of dynamic changes in cerebral oxygenation coupled to neuronal function during mental work in man. *Neurosci. Lett.* **155**:5-8, 1993.

[4] S. Fantini, M. A. Franceschini, J. S. Maier, S. A. Walker, B. Barbieri, and E. Gratton. Frequency-domain multichannel optical detector for noninvasive tissue spectroscopy and oximetry. *Opt. Eng.* **34**:32-42, 1995.

[5] H. Owen-Reece, C. E. Elwell, J. S. Wyatt, and D. T. Delpy. The effect of scalp ischaemia on measurement of cerebral blood volume by near-infrared spectroscopy. *Physiol. Meas.* **17**:279-286, 1996.

[6] M. Wolf, M. Ferrari, and V. Quaresima. Progress of near-infrared spectroscopy and topography for brain and muscle clinical applications. *J. Biomed. Opt.* **12**:062104, 2007.

[7] N. Nagdyman, P. Ewert, B. Peters, O. Miera, T. Fleck, and F. Berger. Comparison of different near-infrared spectroscopic cerebral oxygenation indices with central venous and jugular venous oxygenation saturation in children. *Paediatr. Anaesth.* **18**:160-166, 2008.

[8] P. G. Al-Rawi and P. J. Kirkpatrick. Tissue oxygen index: thresholds for cerebral ischemia using near-infrared spectroscopy. *Stroke* **37**:2720-2725, 2006.

[9] P. B. Benni, B. Chen, F. D. Dykes, S. F. Wagoner, M. Heard, A. J. Tanner, T. L. Young, K. Rais-Bahrami, O. Rivera, and B. L. Short. Validation of the CAS neonatal NIRS system by monitoring vv-ECMO patients: preliminary results. *Adv. Exp. Med. Biol.* **566**:195-201, 2005.

[10] S. E. Nicklin, I. A.-A. Hassan, Y. A. Wickramasinghe, and S. A. Spencer. The light still shines, but not that brightly? The current status of perinatal near infrared spectroscopy. *Arch. Dis. Child. Fetal Neonatal. Ed.* **88**:F263-F268, 2003.

[11] G. Greisen. Is near-infrared spectroscopy living up to its promises? *Semin. Fetal Neonatal. Med.* **11**:498-502, 2006.

[12] F. van Bel, P. Lemmers, and G. Naulaers. Monitoring neonatal regional cerebral oxygen saturation in clinical practice: value and pitfalls. *Neonatology* **94**:237-244, 2008.

[13] D. T. Delpy and M. Cope. Quantification in tissue near-infrared spectroscopy. *Phil. Trans. R. Soc. Lond. B* **352**:649-659, 1997.

[14] Y. Hoshi and M. Tamura. Dynamic multichannel near-infrared optical imaging of human brain activity. *J. Appl. Physiol.* **75**:1842-1846, 1993.

[15] H. Eda, I. Oda, Y. Ito, Y. Wada, Y. Oikawa, Y. Tsunazawa, M. Takada, Y. Tsuchiya, Y. Yamashita, M. Oda, A. Sassaroli, Y. Yamada, and M. Tamura. Multichannel time-resolved optical tomographic imaging system. *Rev. Sci. Instrum.* **70**:3595-3602, 1999.

[16] F. E. W. Schmidt, M. E. Fry, E. M. C. Hillman, J. C. Hebden, and D. T. Delpy. A 32-channel time-resolved instrument for medical optical tomography. *Rev. Sci. Instrum.* **71**:256-265, 2000.

[17] C. H. Schmitz, M. Löcker, J. M. Lasker, A. H. Hielscher, and R. L. Barbour. Instrumentation for fast functional optical tomography. *Rev. Sci. Instrum.* **73**:429-439, 2002.

[18] W. L. Wright. Multimodal monitoring in the ICU: when could it be useful? *J. Neurol. Sci.* **261**:10-15, 2007.

[19] K. E. Wartenberg, J. M. Schmidt, and S. A. Mayer. Multimodality monitoring in neurocritical care. *Crit. Care Clin.* **23**:507-538, 2007.

[20] M. Moseley and G. Donnan. Multimodality imaging. *Stroke* **35**:2632-2634, 2004.

[21] H. Shibasaki. Human brain mapping: hemodynamic response and electrophysiology. *Clin. Neurophysiol.* **119**:731-743, 2008.

[22] D. W. Townsend. Multimodality imaging of structure and function. *Phys. Med. Biol.* **53**:R1-R39, 2008.

[23] E. Niedermeyer and F. L. da Silva. *Electroencephalography: basic principles, clinical applications, and related fields.* **4**th ed., Williams & Wilkins, Baltimore, 1999.

[24] J. S. Wyatt, D. T. Delpy, M. Cope, S. Wray, and E. O. R. Reynolds. Quantification of cerebral oxygenation and haemodynamics in sick newborn infants by near infrared spectrophotometry. *Lancet* **2**:1063-1066, 1986.

[25] C. E. Elwell. *A practical users guide to near infrared spectroscopy.* UCL Reprographics, London, 1995.

[26] C. E. Cooper and R. Springett. Measurement of cytochrome oxidase and mitochondrial energetics by near-infrared spectroscopy. *Phil. Trans. R. Soc. London Ser. B* **352**:669-677, 1997.

[27] H. R. Heekeren, M. Kohl, H. Obrig, R. Wenzel, W. von Pannwitz, S. J. Matcher, U. Dirnagl, C. E. Cooper, and A. Villringer. Noninvasive assessment of changes in cytochrome-c oxidase oxidation in human subjects during visual stimulation. *J. Cereb. Blood Flow Metab.* **19**:592-603, 1999.

[28] M. Kiguchi, N. Ichikawa, H. Atsumori, F. Kawaguchi, H. Sato, A. Maki, and H. Koizumi. Comparison of light intensity on the brain surface due to laser exposure during optical topography and solar irradiation. *J. Biomed. Opt.* **12**:062108, 2007.

[29] A. Villringer and B. Chance. Non-invasive optical spectroscopy and imaging of human brain function. *Trends Neurosci.* **20**:435-442, 1997.

[30] D. M. Rector, R. F. Rogers, J. S. Schwaber, R. M. Harper, and J. S. George. Scattered-light imaging *in vivo* tracks fast and slow processes of neurophysiological activation. *NeuroImage* **14**:977-994, 2001.

[31] E. M. C. Hillman, J. C. Hebden, M. Schweiger, H. Dehghani, F. E. W. Schmidt, D. T. Delpy, and S. R. Arridge. Time resolved optical tomography of the human forearm. *Phys. Med. Biol.* **46**:1117-1130, 2001.

[32] T. Austin, A. P. Gibson, G. Branco, R. Yusof, S. R. Arridge, J. H. Meek, J. S. Wyatt, D. T. Delpy, and J. C. Hebden. Three-dimensional optical imaging of blood volume and oxygenation in the preterm brain. *NeuroImage* **31**:1426-1433, 2006.

[33] P. J. Magistretti, L. Pellerin, D. L. Rothman, and R. G. Shulman. Energy on demand. *Science* **283**:496-497, 1999.

[34] A. Villringer and U. Dirnagl. Coupling of brain activity and cerebral blood flow: basis of functional neuroimaging. *Cerebrovasc. Brain Metab. Rev.* **7**:240-276, 1995.

[35] A. Maiorana, G. O'Driscoll, R. Taylor, and D. Green. Exercise and the nitric oxide vasodilator system. *Sports Med.* **33**:1013-1035, 2003.

[36] M. D. Delp and D. S. O'Leary. Integrative control of the skeletal muscle microcirculation in the maintenance of arterial pressure during exercise. *J. Appl. Physiol.* **97**:1112-1118, 2004.

[37] A. Villringer, J. Planck, C. Hock, L. Schleinkofer, and U. Dirnagl. Near infrared spectroscopy (NIRS): a new tool to study hemodynamic changes during activation of brain function in human adults. *Neurosci. Lett.* **154**:101-104, 1993.

[38] T. J. Huppert, R. D. Hoge, S. G. Diamond, M. A. Franceschini, and D. A. Boas. A temporal comparison of BOLD, ASL, and NIRS hemodynamic responses to motor stimuli in adult humans. *NeuroImage* **29**:368-382, 2006.

[39] S. Ogawa, D. W. Tank, R. Menon, J. M. Ellermann, S. G. Kim, H. Merkle, and K. Ugurbil. Intrinsic signal changes accompanying sensory stimulation: functional brain mapping with magnetic resonance imaging. *Proc. Natl. Acad. Sci. USA* **89**:5951-5955, 1992.

[40] B. R. Rosen, R. L. Buckner, and A. M. Dale. Event-related functional MRI: past, present, and future. *Proc. Natl. Acad. Sci. USA* **95**:773-780, 1998.

[41] P. Fransson, G. Kruger, K. D. Merboldt, and J. Frahm. MRI of functional deactivation: temporal and spatial characteristics of oxygenation-sensitive responses in human visual cortex. *NeuroImage* **9**:611-618, 1999.

[42] F. Kruggel and D. Y. von Cramon. Temporal properties of the hemodynamic response in functional MRI. *Hum. Brain Mapp.* **8**:259-271, 1999.

[43] H. M. Watzman, C. D. Kurth, L. M. Montenegro, J. Rome, J. M. Steven, and S. C. Nicolson. Arterial and venous contributions to near-infrared cerebral oximetry. *Anesthesiology* **93**:947-953, 2000.

[44] E. M. Hillman, A. Devor, M. B. Bouchard, A. K. Dunn, G. W. Krauss, J. Skoch, B. J. Bacskai, A. M. Dale, and D. A. Boas. Depth-resolved optical imaging and microscopy of vascular compartment dynamics during somatosensory stimulation. *NeuroImage* **35**:89-104, 2007.

[45] A. Villringer. Functional neuroimaging: optical approach, *Adv. Exp. Med. Biol.* **413**:1-18, 1997.

[46] R. L. J. Grubb, M. E. Raichle, J. O. Eichling, and M. M. Ter-Pogossian. The effects of changes in PaCO2 on cerebral blood volume, blood flow, and vascular mean transit time. *Stroke* **5**:630-639, 1974.

[47] M. J. Donahue, J. U. Blicher, L. Ostergaard, D. A. Feinberg, B. J. Macintosh, K. L. Miller, M. Günther, and P. Jezzard. Cerebral blood flow, blood volume, and oxygen metabolism dynamics in human visual and motor cortex as measured by whole-brain multi-modal magnetic resonance imaging. *J. Cereb. Blood Flow Metab.* **29**:1856-1866, 2009.

[48] M. A. Franceschini, D. K. Joseph, T. J. Huppert, S. G. Diamond and D. A. Boas. Diffuse optical imaging of the whole head. *J. Biomed. Opt.* **11**:054007, 2006.

[49] M. Ferrari, I. Giannini, G. Sideri, and E. Zanette. Continuous non invasive monitoring of human brain by near infrared spectroscopy. *Adv. Exp. Med. Biol.* **191**:873-882, 1985.

[50] S. J. Matcher, P. Kirkpatrick, K. Nahid, M. Cope, and D. T. Delpy. Absolute quantification methods in tissue near infrared spectroscopy. *Proc. SPIE* **2389**:486-495, 1995.

[51] D. T. Delpy, M. Cope, P. van der Zee, S. Arridge, S. Wray, and J. Wyatt. Estimation of optical pathlength through tissue from direct time of flight measurement. *Phys. Med. Biol.* **33**:1433-1442, 1988.

[52] B. Chance, J. S. Leigh, H. Miyake, D. S. Smith, S. Nioka, R. Greenfeld, M. Finander, K. Kaufmann, W. Levy, M. Young, P. Cohen, H. Yoshioka, and R. Boretsky. Comparison of time resolved and unresolved measurements of deoxyhemoglobin in brain. *Proc. Natn. Acad. Sci. USA* **85**:4971-4975, 1988.

[53] M. Schweiger and S. R. Arridge. Application of temporal filters to time resolved data in optical tomography. *Phys. Med. Biol.* **44**:1699-1717, 1999.

[54] D. Grosenick, H. Wabnitz, H. H. Rinneberg, K. T. Moesta, and P. M. Schlag. Development of a time-domain optical mammograph and first in vivo applications. *Appl. Opt.* **38**:2927-2943, 1999.

[55] J. Selb, D. K. Joseph, and D. A. Boas. Time-gated optical system for depth-resolved functional brain imaging. *J. Biomed. Opt.* **11**:044008, 2006.

[56] J. R. Lakowicz and K. W. Berndt. Frequency domain measurement of photon migration in tissues. *Chem. Phys. Lett.* **166**:246-252, 1990.

[57] B. Chance, M. Cope, E. Gratton, N. Ramanujam, and B. Tromberg. Phase measurement of light absorption and scatter in human tissue. *Rev. Sci. Instrum.* **69**:3457-3481, 1998.

[58] S. R. Arridge, M. Cope, and D. T. Delpy. The theoretical basis for the determination of optical pathlengths in tissue: temporal and frequency analysis. *Phys. Med. Biol.* **37**:1531-1560, 1992.

[59] T. H. Pham, O. Coquoz, J. B. Fishkin, E. Anderson, and B. J. Tromberg. Broad bandwidth frequency domain instrument for quantitative tissue optical spectroscopy. *Rev. Sci. Instrum.* **71**:2500-2513, 2000.

[60] G. Gulsen, B. Xiong, O. Birgul, and O. Nalcioglu. Design and implementation of a multifrequency near-infrared diffuse optical tomography system. *J. Biomed. Opt.* **11**:014020, 2006.

[61] S. R. Arridge and W. R. B. Lionheart. Non-uniqueness in diffusion-based optical tomography. *Opt. Lett.* **23**:882-884, 1998.

[62] V. Ntziachristos, B. Chance, and A. G. Yodh. Differential diffuse optical tomography. *Opt. Express* **5**:230-242, 1999.

[63] E. M. C. Hillman, J. C. Hebden, F. E. W. Schmidt, S. R. Arridge, M. Schweiger, H. Dehghani, and D. T. Delpy. Calibration techniques and datatype extraction for time-resolved optical tomography. *Rev. Sci. Instrum.* **71**:3415-3427, 2000.

[64] C. H. Schmitz, H. L. Graber, H. Luo, I. Arif, J. Hira, Y. Pei, A. Bluestone, S. Zhong, R. Andronica, I. Soller, N. Ramirez, S.-L. S. Barbour, and R. L. Barbour. Instrumentation and calibration protocol for imaging dynamic features in dense-scattering media by optical tomography. *Appl. Opt.* **39**:6466-6486, 2000.

[65] J. C. Hebden, A. Gibson, R. Yusof, N. Everdell, E. M. C. Hillman, D. T. Delpy, S. R. Arridge, T. Austin, J. H. Meek, and J. S. Wyatt. Three-dimensional optical tomography of the premature infant brain. *Phys. Med. Biol.* **47**:4155-4166, 2002.

[66] T. O. McBride, B. W. Pogue, U. L. Osterberg, and K. D. Paulsen. Strategies for absolute calibration of near infrared tomographic tissue imaging. *Adv. Exp. Med. Biol.* **530**:85-99, 2003.

[67] T. Tarvainen, V. Kolehmainen, M. Vauhkonen, A. Vanne, J. P. Kaipio, A. P. Gibson, S. R. Arridge, and M. Schweiger. Computational calibration method for optical tomography. *Appl. Opt.* **44**:1879-1888, 2005.

[68] T. O. McBride, B. W. Pogue, S. Jiang, U. L. Osterberg, and K. D. Paulsen. A parallel-detection frequency-domain near-infrared tomography system for

hemoglobin imaging of the breast in vivo. *Rev. Sci. Instrum.* **72**:1817-1824, 2001.

[69] K.-S. No, R. Kwong, P. H. Chou, and A. Cerussi. Design and testing of a miniature broadband frequency domain photon migration instrument. *J. Biomed. Opt.* **13**:2008.

[70] U. J. Netz, J. Beuthan, and A. H. Hielscher. Multipixel system for gigahertz frequency-domain optical imaging of finger joints. *Rev. Sci. Instrum.* **79**:034301, 2008.

[71] Y. Yang, H. Liu, X. Li, and B. Chance. Low-cost frequency-domain photon migration instrument for tissue spectroscopy, oximetry, and imaging. *Opt. Eng.* **36**:1562-1569, 1997.

[72] N. Ramanujam, C. Du, H. Y. Ma, and B. Chance. Sources of phase noise in homodyne and heterodyne phase modulation devices used for tissue oximetry studies. *Rev. Sci. Instrum.* **69**:3042-3054, 1998.

[73] A. Duncan, J. H. Meek, M. Clemence, C. E. Elwell, L. Tyszchuk, M. Cope, and D. T. Delpy. Optical pathlength measurements on adult head, calf, and forearm and the head of the newborn infant using phase resolved optical spectroscopy. *Phys. Med. Biol.* **40**:295-304, 1995.

[74] I. Nissilä, K. Kotilahti, K. Fallström, and T. Katila. Instrumentation for the accurate measurement of phase and amplitude in optical tomography. *Rev. Sci. Instrum.* **73**:3306-3312, 2002.

[75] I. Nissilä, J. C. Hebden, D. Jennions, J. Heino, M. Schweiger, K. Kotilahti, T. Noponen, A. Gibson, S. Järvenpää, L. Lipiäinen, and T. Katila. A comparison between a time-domain and a frequency-domain system for optical tomography. *J. Biomed. Opt.* **11**:064015, 2006.

[76] K. Kotilahti, I. Nissilä, M. Huotilainen, R. Mäkelä, N. Gavrielides, T. Noponen, P. Björkman, V. Fellman, and T. Katila. Bilateral hemodynamic responses to auditory stimulation in newborn infants. *Neuroreport* **16**:1373-1377, 2005.

[77] H. Radhakrishnan, W. Vanduffel, H. P. Deng, L. Ekstrom, D. A. Boas, and M. A. Franceschini. Fast optical signal not detected in awake behaving monkeys. *NeuroImage* **45**:410-419, 2009.

[78] N. Roche-Labarbe, S. A. Carp, A. Surova, M. Patel, D. A. Boas, P. E. Grant, and M. A. Franceschini. Noninvasive optical measures of CBV, StO(2), CBF

index, and rCMRO(2) in human premature neonates' brains in the first six weeks of life. *Hum. Brain Mapp.,* 2009. (In press)

[79] K. Kotilahti, I. Nissilä, T. Näsi, L. Lipiäinen, T. Noponen, P. Meriläinen, M. Huotilainen, and V. Fellman. Hemodynamic responses to speech and music in newborn infants. *Hum. Brain Mapp.,* 2009. (In press)

[80] S. J. Matcher, C. E. Elwell, C. E. Cooper, M. Cope, and D. T. Delpy. Performance comparison of several published tissue near-infrared spectroscopy algorithms. *Anal. Biochem.* **227**:54-68, 1995.

[81] A. Sassaroli and S. Fantini. Comment on the modified Beer-Lambert law for scattering media. *Phys. Med. Biol.* **49**:N255-N257, 2004.

[82] G. Strangman, M. A. Franceschini, and D. A. Boas. Factors affecting the accuracy of near-infrared spectroscopy concentration calculations for focal changes in oxygenation parameters. *NeuroImage* **18**:865-879, 2003.

[83] M. S. Patterson, B. Chance, and B. C. Wilson. Time resolved reflectance and transmittance for the non-invasive measurement of tissue optical properties. *Appl. Opt.* **28**:2331-2336, 1989.

[84] J. B. Fishkin and E. Gratton. Propagation of photon-density waves in strongly scattering media containing an absorbing semi-infinite plane bounded by a straight edge. *J. Opt. Soc. Am. A* **10**:127-140, 1993.

[85] S. Fantini, M. A. Franceschini, J. B. Fishkin, B. Barbieri, and E. Gratton. Quantitative determination of the absorption spectra of chromophores in strongly scattering media: a light-emitting-diode based technique. *Appl. Opt.* **33**:5204-5213, 1994.

[86] S. Fantini, M. A. Franceschini, and E. Gratton. Semi- infinite-geometry boundary problem for light migration in highly scattering media: a frequency-domain study in the diffusion approximation. *J. Opt. Soc. Am. B* **11**:2128-2138, 1994.

[87] H. Liu, D. A. Boas, Y. Zhang, A. G. Yodh, and B. Chance. Determination of optical properties and blood oxygenation in tissue using continuous NIR light. *Phys. Med. Biol.* **40**:1983-1993, 1995.

[88] M. A. Franceschini, S. Thaker, G. Themelis, K. K. Krishnamoorthy, H. Bortfeld, S. G. Diamond, D. A. Boas, K. Arvin, and P. E. Grant. Assessment of infant brain development with frequency-domain near-infrared spectroscopy. *Pediatr. Res.* **61**:546-551, 2007.

[89] H. Koizumi, T. Yamamoto, A. Maki, Y. Yamashita, H. Sato, H. Kawaguchi, and N. Ichikawa. Optical topography: Practical problems and new applications. *Appl. Opt.* **42**:3054-3062, 2003.

[90] J. Steinbrink, H. Wabnitz, H. Obrig, A. Villringer, and H. Rinneberg. Determining changes in NIR absorption using a layered model of the human head. *Phys. Med. Biol.* **46**:879-896, 2001.

[91] F. Martelli, A. Sassaroli, Y. Yamada, and G. Zaccanti. Analytical approximate solutions of the time-domain diffusion equation in layered slabs. *J. Opt. Soc. Am. A* **19**:71-80, 2002.

[92] E. Okada and D. T. Delpy. Near-infrared light propagation in an adult head model. II. Effect of superficial tissue thickness on the sensitivity of the near-infrared spectroscopy signal. *Appl. Opt.* **42**:2915-2922, 2003.

[93] S. R. Arridge. Optical tomography in medical imaging. *Inverse Probl.* **15**:41-93, 1999.

[94] F. A. Rasulo, E. De Peri, and A. Lavinio. Transcranial Doppler ultrasonography in intensive care. *Eur. J. Anaesthesiol. Suppl.* **42**:167-173, 2008.

[95] S. L. Watkin, S. A. Spencer, P. W. Dimmock, Y. A. B. D. Wickramasinghe, and P. Rolfe. A comparison of pulse oximetry and near infrared spectroscopy (NIRS) in the detection of hypoxaemia occurring with pauses in nasal airflow in neonates. *J. Clin. Monit. Comput.* **15**:441-447, 1999.

[96] Y. Hoshi, S. Mizukami, and M. Tamura. Dynamic features of hemodynamic and metabolic changes in the human brain during all-night sleep as revealed by near-infrared spectroscopy. *Brain Research* **652**:257-262, 1994.

[97] A. Spielman, G. Zhang, C. M. Yang, P. D'Ambrosio, S. Serizawa, M. Nagata, H. von Gizycki, and R. Alfano. Intracerebral hemodynamics probed by near infrared spectroscopy in the transition between wakefulness and sleep. *Brain Research* **866**:313-325, 2000.

[98] M. Uchida-Ota, N. Tanaka, H. Sato H, and A. Maki. Intrinsic correlations of electroencephalography rhythms with cerebral hemodynamics during sleep transitions. *NeuroImage* **42**:357-368, 2008.

[99] T. Noponen. *Instrumentation for diffuse optical imaging in the frequency domain.* Master's thesis, Helsinki University of Technology, 2001. (in Finnish)

[100] T. Noponen. *Instrumentation for diffuse optical imaging and near-infrared spectroscopy and their applications in human brain studies.* Licentiate thesis, Helsinki University of Technology, 2004.

[101] M. A. Franceschini, E. Gratton, and S. Fantini. Non-invasive optical method to measure tissue and arterial saturation: an application to absolute pulse oximetry of the brain. *Opt. Lett.* **24**:829-831, 1999.

[102] N. Gavrielides. *Extending a frequency domain optical tomography system for the functional imaging of the infant brain.* Master's thesis, Helsinki University of Technology, 2006.

[103] K. G. Libbrecht and J. L. Hall. A low-noise high-speed diode laser current controller. *Rev. Sci. Instrum.* **64**:2133-2135, 1993.

[104] K. Kotilahti. *Optical imaging of brain activation.* Master's thesis, Helsinki University of Technology, 2001. (in Finnish)

[105] F. G. Shellock and E. Kanal. *Magnetic Resonance: Bioeffects, Safety, and Patient Management.* Second Edition, Lippincott-Raven Press, New York, 1996.

[106] R. J. Ilmoniemi, J. Ruohonen, and J. Karhu. Transcranial magnetic stimulation − a new tool for functional imaging of the brain. *Crit. Rev. Biomed. Eng.* **27**:241-284, 1999.

[107] D. W. Swanson and L. R. Enlow. Stress effects of epoxy adhesives on ceramic substrates and magnetics. *Microelectronics Reliability* **41**:499-510, 1999.

[108] J. F. Nunn. *Applied respiratory physiology.* Butterworths, London, 1987.

[109] L. Qin, P. van Gelderen, J. A. Derbyshire, F. Jin, J. Lee, J. A. de Zwart, Y. Tao, and J. H. Duyn. Prospective head-movement correction for high-resolution MRI using an in-bore optical tracking system. *Magn. Reson. Med.* **62**:924-934, 2009.

[110] P. M. Bloomfield, T. J. Spinks, J. Reed, L. Schnorr, A. M. Westrip, L. Livieratos, R. Fulton, and T. Jones. The design and implementation of a motion correction scheme for neurological PET. *Acad. Radiol.* **13**:1093-1103, 2006.

[111] D. T. Wehner, M. S. Hämäläinen, M. Mody, and S. P. Ahlfors. Head movements of children in MEG: quantification, effects on source estimation, and compensation. *NeuroImage* **40**:541-550, 2008.

[112] M. Izzetoglu, A. Devaraj, S. Bunce, and B. Onaral. Motion artifact cancellation in NIR spectroscopy using Wiener filtering. *IEEE Trans. Biomed. Eng.* **52**:934-938, 2005.

[113] H. Sato, N. Tanaka, M. Uchida, Y. Hirabayashi, M. Kanai, T. Ashida, I. Konishi, and A. Maki. Wavelet analysis for detecting body-movement artifacts in optical topography signals. *NeuroImage* **33**:580-587, 2006.

[114] T. J. Farrell, M. S. Patterson, and B. Wilson. A diffusion theory model of spatially resolved, steady-state diffuse reflectance for the noninvasive determination of tissue optical properties in vivo. *Med. Phys.* **19**:879-888, 1992.

[115] S. Suzuki, S. Takasaki, T. Ozaki, and Y. Kobayashi Y. A tissue oxygenation monitor using NIR spatially resolved spectroscopy. *Proc. SPIE* **3597**:582-592, 1999.

[116] S. J. Matcher, M. Cope, and D. T. Delpy. In vivo measurements of the wavelength dependence of tissue-scattering coefficients between 760 and 900 nm measured with time-resolved spectroscopy. *Appl. Opt.* **36**:386-396, 1997.

[117] H. Obrig, M. Neufang, R. Wenzel, M. Kohl, J. Steinbrink, K. M. Einhäupl, and A. Villringer. Spontaneous low frequency oscillations of cerebral hemodynamics and metabolism in human adults. *NeuroImage* **12**:623-639, 2000.

[118] S. R. Seydnejad and R. I. Kitney. Modeling of Mayer waves generation mechanisms. *IEEE Eng. Med. Biol. Mag.* **20**:92-100, 2001.

[119] C. E. Elwell, R. Springett, E. Hillman, and D. T. Delpy. Oscillations in cerebral haemodynamics - implications for functional activation studies. *Adv. Exp. Med. Biol.* **471**:57-65, 1999.

[120] J. C. T. Pepperell, R. J. O. Davies, and J. R. Stradling. Sleep studies for sleep apnoea. *Physiol. Meas.* **23**:R39-R74, 2002.

[121] J. R. Stradling and R. J. O. Davies. Is it necessary to record sleep? *Sleep* **19**:S251-S254, 1996.

[122] W. W. Flemons and J. E. Remmers. The diagnosis of sleep apnea: questionnaires and home studies. *Sleep* **19**:S243-S247, 1996.

[123] A. Sadeh, P. J. Hauri, D. F. Kripke, and P. Lavie. The role of actigraphy in the evaluation of sleep disorders. *Sleep* **18**:288-302, 1995.

[124] P. J. E. Vos and J. R. Stradling. Assessment of sleep times and movement arousals from video recordings. *J. Amb. Mon.* **4**:35-42, 1991.

[125] J. Empson. *Sleep and dreaming.* Faber and Faber, London, 1990.

[126] P. Maquet. Functional neuroimaging of normal human sleep by positron emission tomography. *J. Sleep Res.* **9**:207-231, 2000.

[127] A. Rechtschaffen and A. Kales. *A manual of standardized terminology, techniques, and scoring system for sleep stages of human subjects.* National Institutes of Health, Publication No. **204**, US Government Printing Office, US Public Health Service, 1968.

[128] P. van der Zee, M. Cope, S. R. Arridge, M. Essenpreis, L. A. Potter, and A. D. Edwards. Experimentally measured optical pathlengths for the adult head, calf and forearm and the head of the newborn infant as a function of interoptode spacing. *Adv. Exp. Med. Biol.* **316**:143-153, 1992.

[129] G. Bonmassar, N. Hadjikhani, J. R. Ives, D. Hinton, and J. W. Belliveau. Influence of EEG electrodes on the BOLD fMRI signal. *Hum. Brain Mapp.* **14**:108-115, 2001.

[130] C. J. Scarff, A. Reynolds, B. G. Goodyear, C. W. Ponton, J. C. Dort, and J. J. Eggermont. Simultaneous 3-T fMRI and high-density recording of human auditory evoked potentials. *NeuroImage* **23**:1129-1142, 2004.

[131] C. Mulert, L. Jager, R. Schmitt, P. Bussfeld, O. Pogarell, H. J. Moller, G. Juckel, and U. Hegerl. Integration of fMRI and simultaneous EEG: towards a comprehensive understanding of localization and time-course of brain activity in target detection. *NeuroImage* **22**:83-94, 2004.

[132] R. P. Kennan, S. G. Horovitz, A. Maki, Y. Yamashita, H. Koizumi, and J. C. Gore. Simultaneous recording of event-related auditory oddball response using transcranial near infrared optical topography and surface EEG. *NeuroImage* **16**:587-592, 2002.

[133] H. Obrig, H. Israel, M. Kohl-Bareis, K. Uludag, R. Wenzel, B. Muller, G. Arnold, and A. Villringer. Habituation of the visually evoked potential and its vascular response: implications for neurovascular coupling in the healthy adult. *NeuroImage* **17**:1-18, 2002.

[134] M. Moosmann, P. Ritter, I. Krastel, A. Brink, S. Thees, F. Blankenburg, B. Taskin, H. Obrig, and A. Villringer. Correlates of alpha rhythm in functional magnetic resonance imaging and near infrared spectroscopy. *NeuroImage* **20**:145-158, 2003.

[135] S. G. Horovitz and J. C. Gore. Simultaneous event-related potential and near-infrared spectroscopic studies of semantic processing. *Hum. Brain Mapp.* **22**:110-115, 2004.

[136] S. P. Koch, J. Steinbrink, A. Villringer, and H. Obrig. Synchronization between background activity and visually evoked potential is not mirrored by focal hyperoxygenation: implications for the interpretation of vascular brain imaging. *J. Neurosci.* **26**:4940-4948, 2006.

[137] L. Rovati, G. Salvatori, L. Bulf, and S. Fonda. Optical and electrical recording of neural activity evoked by graded contrast visual stimulus. *BioMed. Eng. Online* **6**:28, 2007.

[138] M. J. Herrmann, T. Huter, M. Plichta, A. C. Ehlis, G. W. Alpers, A. Muhlberger, and A. J. Fallgatter. Enhancement of activity of the primary visual cortex during processing of emotional stimuli as measured with event-related functional near-infrared spectroscopy and event related potentials. *Hum. Brain Mapp.* **29**:28-35, 2008.

[139] S. P. Koch, S. Koendgen, R. Bourayou, J. Steinbrink, and H. Obrig. Individual alpha-frequency correlates with amplitude of visual evoked potential and hemodynamic response. *NeuroImage* **41**:233-242, 2008.

[140] T. Näsi, K. Kotilahti, T. Noponen, I. Nissilä, L. Lipiäinen, and P. Meriläinen. Correlation of visual evoked hemodynamic responses and potentials in human brain. *Exp. Brain Res.,* 2009. (Accepted)

[141] J. Virtanen, J. Ruohonen, R. Näätänen, and R. J. Ilmoniemi. Instrumentation for the measurement of electric brain responses to transcranial magnetic stimuli. *Med. Biol. Eng. Comput.* **37**:322-326, 1999.

[142] G. F. A. Harding, J. V. Odom, W. Spileers, and H. Spekreijse. Standard for visual evoked potentials 1995. *Vision Res.* **36**:3567-3572, 1995.

[143] J. R. Fineman, S. J. Soifer, and M. A. Heymann. Regulation of pulmonary vascular tone in the perinatal period. *Annu. Rev. Physiol.* **57**:115-134, 1995.

[144] American Academy of Pediatrics. Committee on Fetus and Newborn. Use of inhaled nitric oxide. *Pediatrics* **106**:344-345, 2000.

[145] M. H. Zou and V. Ullrich. Peroxynitrite formed by simultaneous generation of nitric oxide and superoxide selectively inhibits bovine aortic prostacyclin synthase. *FEBS Lett.* **382**:101-104, 1996.

[146] M. Ehlen and B. Wiebe. Iloprost in persistent pulmonary hypertension of the newborn. *Cardiol. Young* **13**:361-363, 2003.

[147] V. Lambert, A. Serraf, P. Durand, and J. Losay. Aerosolized iloprost therapy in an infant with chronic pulmonary hypertension after a neonatal arterial switch operation. *Arch. Pediatr.* **8**:1218-1221, 2001.

[148] K. Olmsted, O. Oluola, A. Parthiban, and T. Raghuveer T. Can inhaled prostacyclin stimulate surfactant in ELBW infants? *J. Perinatol.* **27**:724-726, 2007.

[149] M. De Vroomen, P. Steendijk, R. H. Lopes Cardozo, H. H. Brouwers, F. Van Bel, and J. Baan. Enhanced systolic function of the right ventricle during respiratory distress syndrome in newborn lambs. *Am. J. Physiol. Heart Circ. Physiol.* **280**:H392-H400, 2001.

[150] V. Perez-de-Sa, D. Cunha-Goncalves, A. Nordh, S. Hansson, A. Larsson, D. Ley, V. Fellman, and O. Werner. High brain tissue oxygen tension during ventilation with 100% oxygen after fetal asphyxia in newborn sheep. *Pediatr. Res.* **65**:57-61, 2009.

[151] K. A. Marks, E. C. Mallard, I. Roberts, C. E. Williams, E. S. Sirimanne, B. Johnston, P. D. Gluckman, and A. D. Edwards. Delayed vasodilation and altered oxygenation after cerebral ischemia in fetal sheep. *Pediatr. Res.* **39**:48-54, 1996.

[152] D. A. Boas, T. J. Gaudette, and S. R. Arridge. Simultaneous imaging and optode calibration with diffusive optical tomography. *Opt. Express* **8**:263-270, 2001.

[153] M. Schweiger, I. Nissilä, D. A. Boas, and S. R. Arridge. Image reconstruction in optical tomography in the presence of coupling errors. *Appl. Opt.* **46**:2743-2756, 2007.

[154] B. W. Pogue and M. S. Patterson. Frequency-domain optical absorption spectroscopy of finite tissue volumes using diffusion theory. *Phys. Med. Biol.* **39**:1157-1180, 1994.

[155] R. C. Haskell, L. O. Svaasand, T.-T. Tsay, T.-C. Feng, M. S. McAdams, and B. J. Tromberg. Boundary conditions for the diffusion equation in radiative transfer. *J. Opt. Soc. Am. A* **11**:2727-2741, 1994.

[156] F. Martelli, D. Contini, A. Taddeucci, and G. Zaccanti. Photon migration through a turbid slab described by a model based on diffusion approximation. II. Comparison with Monte Carlo results. *Appl. Opt.* **36**:4600-4612, 1997.

[157] M. Gerken and G. W. Faris. High-precision frequency-domain measurements of the optical properties of turbid media. *Opt. Lett.* **24** 930-932, 1999.

[158] B. W. Pogue, K. D. Paulsen, C. Abele, and H. Kaufman. Calibration of near-infrared frequency-domain tissue spectroscopy for absolute absorption coefficient quantitation in neonatal head-simulating phantoms. *J. Biomed. Opt.* **5**:185-193, 2000.

[159] F. Martelli, M. Bassani, L. Alianelli, L. Zangheri, and G. Zaccanti. Accuracy of the diffusion equation to describe photon migration through an infinite medium: numerical and experimental investigation. *Phys. Med. Biol.* **45**:1359-1373, 2000.

[160] G. Zaccanti, S. Del Bianco, and F. Martelli. Measurements of optical properties of high-density media. *Appl. Opt.* **42**:4023-4030, 2003.

[161] F. Martelli and G. Zaccanti. Calibration of scattering and absorption properties of a liquid diffusive medium at NIR wavelengths. CW method. *Opt. Express* **15**:486-500, 2007.

[162] S. Fantini, M. A. Franceschini, and E. Gratton. Effective source term in the diffusion equation for photon transport in turbid media. *Appl. Opt.* **36**:156-163, 1997.

[163] V. Venugopalan, J. S. You, and B. J. Tromberg. Radiative transport in the diffusion approximation: An extension for highly absorbing media and small source-detector separations. *Phys. Rev. E* **58**:2395-2407, 1998.

[164] M. Hiraoka, M. Firbank, M. Essenpreis, M. Cope, S. R. Arridge, P. van der Zee, and D. T. Delpy. A Monte Carlo investigation of optical pathlength in inhomogeneous tissue and its application to near-infrared spectroscopy. *Phys. Med. Biol.* **38**:1859-1876, 1993.

[165] T. J. Germon, P. D. Evans, A. R. Manara., N. J. Barnett, P. Wall, and R. J. Nelson. Sensitivity of near infrared spectroscopy to cerebral and extracerebral oxygenation changes is determined by emitter-detector separation. *J. Clin. Monit. Comput.* **14**:353-360, 1998.

[166] J. Virtanen, T. Noponen, and P. Meriläinen. Comparison of principal and independent component analysis in removing extracerebral interference from near-infrared spectroscopy signals. *J. Biomed. Opt.* **14**:054032, 2009.

[167] J. C. Hebden and T. Austin. Optical tomography of the neonatal brain. *Eur. Radiol.* **17**:2926-2933, 2007.

[168] H. Zhao, F. Gao, Y. Tanikawa, and Y. Yamada. Time-resolved diffuse optical tomography and its application to *in vitro* and *in vivo* imaging. *J. Biomed. Opt.* **12**:062107, 2007.

[169] M. Toiviainen. *Intermediate frequency amplifier for a frequency domain optical tomography instrument*. Special assignment, Helsinki University of Technology, 2009.

[170] J. Virtanen. *Near-infrared spectroscopy in measuring changes of cerebral haemoglobin concentrations during natural sleep.* Master's thesis, Helsinki University of Technology, 2007.

[171] T. Näsi, K. Kotilahti, H. Mäki, I. Nissilä, and Pekka Meriläinen. Combining near-infrared spectroscopy with electroencephalography and repetitive transcranial magnetic stimulation. *European Conferences on Biomedical Optics.* Munich, Germany, 14 − 18 June, 2009.

[172] L. P. Safonova, A. Michalos, U. Wolf, M. Wolf, D. M. Hueber, J. H. Choi, R. Gupta, C. Polzonetti, W. W. Mantulin, and E. Gratton. Age-correlated changes in cerebral hemodynamics assessed by near-infrared spectroscopy. *Arch. Gerontol. Geriatr.* **39**: 207-225, 2004.

[173] W. Liboni, F. Molinari, G. B. Allais, O. Mana, E. Negri, G. D'Andrea, G. Bussone, and C. Benedetto. Patent foramen ovale detected by near-infrared spectroscopy in patients suffering from migraine with aura. *Neurol. Sci.* **29**(Suppl 1):S182-185, 2008.

[174] S. Magon, G. Basso, P. Farace, G. K. Ricciardi, A. Beltramello, and A. Sbarbati. Reproducibility of BOLD signal change induced by breath holding. *NeuroImage* **45**:702-712, 2009.

[175] G. Themelis, H. D'Arceuil, S. G. Diamond, S. Thaker, T. J. Huppert, D. A. Boas, and M. A. Franceschini. Near-infrared spectroscopy measurement of the pulsatile component of cerebral blood flow and volume from arterial oscillations. *J. Biomed. Opt.* **12**:014033, 2007.

[176] D. A. Boas, G. Strangman, J. P. Culver, R. D. Hoge, G. Jasdzewski, R. A. Poldrack, B. R. Rosen, and J. B. Mandeville. Can the cerebral metabolic rate of oxygen be estimated with near-infrared spectroscopy? *Phys. Med. Biol.* **48**:2405-2418, 2003.

[177] Y. Hoshi, S. Kosaka, Y. Xie, S. Kohri, and M. Tamura. Relationship between fluctuations in the cerebral hemoglobin oxygenation state and neuronal activity under resting conditions in man. *Neurosci. Lett.* **245**:147-150, 1998.

[178] I. Tachtsidis, C. E. Elwell, T. S. Leung, C.-W. Lee, M. Smith, and D. T. Delpy. Investigation of cerebral haemodynamics by near-infrared spectroscopy in young healthy volunteers reveals posture-dependent spontaneous oscillations. *Physiol. Meas.* **25**:437-445, 2004.

[179] R. L. Barbour, H. L. Graber, Y. Pei, S. Zhong, and C. H. Schmitz. Optical tomographic imaging of dynamic features of dense-scattering media. *J. Opt. Soc. Am. A* **18**:3018-3036, 2001.

[180] S. G. Diamond, T. J. Huppert, V. Kolehmainen, M. A. Franceschini, J. P. Kaipio, S. R. Arridge, and D. A. Boas. Dynamic physiological modeling for functional diffuse optical tomography. *NeuroImage* **30**:88-101, 2006.

[181] P. Sleight and B. Casadei. Relationships between heart rate, respiration, and blood pressure variabilities. In M. Malik and A. J. Camm, eds. *Heart Rate Variability.* Futura Pub. Co., pp. 311-327, 1995.

[182] K. Iwasaki, Y. Ogawa, S. Shibata, and K. Aoki. Acute exposure to normobaric mild hypoxia alters dynamic relationships between blood pressure and cerebral blood flow at very low frequency. *J. Cereb. Blood Flow Metab.* **27**:776-784, 2007.

[183] T. Katura, N. Tanaka, A. Obata, H. Sato, and A. Maki. Quantitative evaluation of interrelations between spontaneous low-frequency oscillations in cerebral hemodynamics and systemic cardiovascular dynamics. *NeuroImage* **31**:1592-1600, 2006.

[184] T. Hayakawa, M. Terahima, Y. Kayukawa, T. Ohta, and T. Okada. Changes in cerebral oxygenation and hemodynamics during obstructive sleep apneas. *Chest* **109**:916-921, 1996.

[185] A. D. McGown, H. Makker, C. Elwell, P. G. Al-Rawi, A. Valipour, and S. G. Spiro. Measurement of changes in cytochrome oxidase redox state during obstructive sleep apnea using near-infrared spectroscopy. *Sleep* **26**:710-716, 2003.

[186] P. Lapinlampi. *Assessment of the depth of natural sleep with Datex-Ohmeda S/5^{TM} Entropy Module.* Special assignment, Helsinki University of Technology, 2005.

[187] R. J. Cooper, N. L. Everdell, L. C. Enfield, A. P. Gibson, A. Worley, and J. C. Hebden. Design and evaluation of a probe for simultaneous EEG and near-infrared imaging of cortical activation. *Phys. Med. Biol.* **54**:2093-2102, 2009.

[188] B. M. Mackert, G. Wubbeler, S. Leistner, K. Uludag, H. Obrig, A. Villringer, L. Trahms, and G. Curio. Neurovascular coupling analyzed non-invasively in the human brain. *Neuroreport* **15**:63-66, 2004.

[189] W. Ou, I. Nissilä, H. Radhakrishnan, D. A. Boas, M. S. Hämäläinen, and M. A. Franceschini. Study of neurovascular coupling in humans via simultaneous magnetoencephalography and diffuse optical imaging acquisition. *NeuroImage* **46**:624-632, 2009.

[190] P. Smielewski, P. Kirkpatrick, P. Minhas, J. D. Pickard, and M. Czosnyka. Can cerebrovascular reactivity be measured with near-infrared spectroscopy? *Stroke* **26**:2285-2292, 1995.

[191] S. S. Dixit, H. Kim, B. Visser, and G. W. Faris. Development of a transillumination infrared modality for differential vasoactive optical imaging. *Appl. Opt.* **48**:178-186, 2009.

[192] L. J. Kemna and S. Posse. Effect of respiratory CO(2) changes on the temporal dynamics of the hemodynamic response in functional MR imaging. *NeuroImage* **14**:642-649, 2001.

[193] S. Posse, L. J. Kemna, B. Elghahwagi, S. Wiese, and V. G. Kiselev. Effect of graded hypo- and hypercapnia on fMRI contrast in visual cortex: quantification of T(*)(2) changes by multiecho EPI. *Magn. Reson. Med.* **46**:264-271, 2001.

[194] H. D. Davies, W. M. Carroll, and F. L. Mastaglia. Effects of hyperventilation on pattern-reversal visual evoked potentials in patients with demyelination. *J. Neurol. Neurosurg. Psychiatry* **49**:1392-1396, 1986.

[195] J. Bednarik and O. Novotny. Value of hyperventilation in pattern-reversal visual evoked potentials. *J. Neurol. Neurosurg. Psychiatry* **52**:1107-1109, 1989.

[196] V. S. Gavriysky. Influence of a twofold voluntary hyperventilation on visually evoked cortical potentials and human pupillogram. *Doc. Ophthalmol.* **77**:213-224, 1991.

[197] Y. Minagawa-Kawai, K. Mori, J. C. Hebden, and E. Dupoux. Optical imaging of infants' neurocognitive development: recent advances and perspectives. *Developmental Neurobiology* **68**:712-728, 2008.

[198] J. Choi, M. Wolf, V. Toronov, U. Wolf, C. Polzonetti, D. Hueber, L. P. Safonova, R. Gupta, A. Michalos, W. Mantulin, and E. Gratton. Noninvasive determination of the optical properties of adult brain: near-infrared spectroscopy approach. *J. Biomed. Opt.* **9**:221-229, 2004.

[199] C. E. Cooper, C. E. Elwell, J. H. Meek, S. J. Matcher, J. S. Wyatt, M. Cope, and D. T. Delpy. The noninvasive measurement of absolute cerebral deoxyhemoglobin concentration and mean optical path length in the neonatal brain by second derivative near infrared spectroscopy. *Pediatr. Res.* **39**:32-38, 1996.

ISBN 978-952-248-210-5
ISBN 978-952-248-211-2 (PDF)
ISSN 1795-2239
ISSN 1795-4584 (PDF)